TÉCNICO LISBOA

Looking for Coherence Effects in the Quark-Gluon Plasma

João Diogo Mesquita Lopes

Thesis to obtain the Master of Science Degree in

Engineering Physics

Supervisors: Prof. Dr. Liliana Marisa Cunha Apolinário
Prof. Dr. Leticia Cunqueiro Mendez

Examination Committee

Chairperson: Prof. Dr. Mário João Martins Pimenta
Supervisor: Prof. Dr. Leticia Cunqueiro Mendez
Member of the Committee: Prof. Dr. Patrícia Conde Muíño

October 2022

Yesterday I was clever, so I wanted to change the world.

Today I am wise, so I am changing myself.

Rumi

Acknowledgements

First I would like to thank my supervisors Liliana and Leticia. Without them none of this project would have seen the light of day. Both were extremely patient and thoughtful even when I, most likely, did not deserve such care. A special note to Liliana who accompanied me during my academic path at IST since the begging until the very end and was always across the hallway ready to help.

Next I would like to thank my friends and colleagues. "The night was dark and full of terrors" and we spent many nights of terror together so here is a thank you remark for helping me during the past five years. We laughed a lot, we cried a lot but in the end only the laughter mattered and it will be only the fun moments that will endure.

E agora em português, um agradecimento muito especial à minha familia. Primeiro aos meus pais pelo apoio incondicional nas horas boas e nas horas más, por estarem sempre lá quando tudo parecia estar perdido. Ah e claro tenho muito que lhes agradecer por terem sido os grandes sponsors desta viagem que agora termina (e de todas as viagens que fiz pelo meio). À Sofia por me ajudar a ver o mundo de forma diferente e me manter motivado. Aos meus avós que nunca me faltaram e sempre têm uma palavra amiga e de encorajamento.

Por último tenho que agradecer à Sara. A Sara apareceu a meio caminho deste projeto, mas apareceu na altura certa. Sem ela esta dissertação muito provavelmente não estaria pronta a tempo. A Sara é a minha maior fã (e ela sabe que eu sou o dela). A Sara está sempre a uma chamada de distância quando "os plots estão todos mal". A Sara tem sempre um "vai dar tudo certo" no bolso para me oferecer. A Sara é a Sara e por isso tenho que lhe agradecer.

Seria um pouco hipócrita da minha parte se, passados 5 anos no Técnico, apenas escrevesse coisas boas relativamente à minha passagem por esta instituição. Não, não foi um mar de rosas. Não, o Mestrado Integrado em Engª Física Tecnológica (como se chamava em 2017/2018) não é nada fácil; talvez nunca venha a ter uma provação tão grande no resto da vida em termos de pressão psicológica e intelectual. Mas mesmo assim, talvez deva um agradecimento ao Técnico. Bati muitas vezes com a cabeça na parede, encontrei muitas dificuldades talvez desnecessariamente proporcionadas pela própria instituição. Mas o que é certo é que agora acabou e dessas provações que o Técnico me proporcionou só tenho a agradecer os amigos que me deu e a capacidade mental e psicológica que adquiri ao aderir à política do "desenrascanço". Isso e o aprender que nada se faz sozinho e que se queres alguma coisa tens de ir lá tirá-la, caso contrário ninguém te dá nada. Fiz muita coisa, vi muita coisa, aprendi algumas coisas pelo meio e por isso só posso dizer: Obrigado, Técnico.

Resumo

O observável jet pull fornece informação relativamente ao fluxo de cor estabelecido entre dois jatos interconectados, adicionalmente à habitualmente obtida através do momento e do tamanho dos jatos. Apesar das correlações de cor já terem sido estudadas anteriormente, propomo-nos desenvolver uma nova abordagem: aplicar o vetor jet pull em coerência intra-jato. Para tal, estudamos simulações de eventos protão-protão a energias de centro de massa semelhantes às do Large Hadron Collider: $\sqrt{s} = 5$ TeV e $\sqrt{s} = 13$ TeV. Nestes eventos, definimos singletos e octetos de cor, através do duplo decaimento fraco de bosões e de eventos QCD, respetivamente. Definimos o observável pull angle num sistema di-jato formado através de técnicas de reconstrução anti-k_T de jatos e de substrutura de jatos. O objetivo consiste em testar se os sinais relacionados com coerência de cor se mantém em ambiente de colisões de iões pesados. Ainda exploramos o decaimento do glião num par $c\bar{c}$, através de mesões D. Finalmente, adicionamos um background térmico aos três sistemas, tendo este características semelhantes às do background de uma colisão Pb-Pb a $\sqrt{s} = 5.02$ TeV. O background provoca alterações significativas ao comportamento do singleto e do octeto $c\bar{c}$. Dessa forma, aplicamos uma subtração de background ao nivel dos constituintes, semelhante à utilizada nas experiências. Isto permite obter novamente a assinatura obtida em eventos pp em vácuo, provando que os efeitos de coerência de cor podem ser testados em colisões de iões pesados.

Palavras-chave: Pull-vector; Coerência; Background; Jato; Singleto; Octeto

Abstract

The jet pull observable supplies additional information regarding the colour flow between interconnected jets, besides momentum and size, usually used to study such objects. Previous work was performed to study the colour correlation between colour singlet jets. We aim to set the baseline for a new approach: apply jet pull to intra-jet (de)coherence. For that, we study simulated proton-proton events at the same centre-of-mass energies as the Large Hadron Collider: $\sqrt{s} = 5$ TeV and $\sqrt{s} = 13$ TeV. In these events, we define colour singlet and octet jet topologies through double boson weak decay and hard QCD events, respectively. The observable pull angle is then defined in a di-jet system formed by using either fully reclustered anti-k_T jets or jet substructure techniques. Our motivation is to test whether signals related with colour coherence effects stand in an heavy ion collision environment. The gluon splitting into a $c\bar{c}$ pair was also explored, by tagging D-mesons in a realistic scenario. Finally, we embedded these three systems in a thermal background with settings alike the background of Pb-Pb collisions at $\sqrt{s} = 5.02$ TeV. The background distorts the observable significantly and we apply a constituent subtraction approach, similar to the one available at the collider experiments, to subtract its effect on average. We retrieve the signal seen in a vacuum pp events, proving that the colour coherence effects will be possible to test in heavy-ion events.

Keywords: Pull Vector; Coherence; Background; Jets; Singlet; Octet

Table of Contents

List of Tables

List of Figures

List of Symbols

Greek symbols

γ^{μ}	Dirac matrix.
μ, ν, σ	Spacetime indices.

Roman symbols

$\mathscr{L}$	Lagrangian, or lagrangian density.
f^{abc}	SU(N) structure functions.
T^{a}_{ij}	SU(N) generator.

Subscripts

i, j, k	Colour indices pertaining to the fundamental representation.

Superscripts

a, b, c	Colour indices pertaining to the adjoint representation.

Other

∂_{μ}	Partial derivative.

List of Abbreviations

AA nucleus-nucleus.

C/A Cambridge-Aachen.

CERN Conseil Européen pour la Recherche Nucléaire.

FF Fragmentation Function.

HIC Heavy Ion Collision.

LHC Large Hadron Collider.

PDF Parton Distribution Function.

pp proton-proton.

pQCD Perturbative Quantum Chromodynamics.

QCD Quantum Chromodynamics.

QGP Quark-Gluon Plasma.

RHIC Relativistic Heavy Ion Collider.

Chapter 1

Introduction

1.1 Particle Physics Standard Model and QCD

We live surrounded by matter. As well as cells are the elementary pieces of the human body, matter has its own elementar constituents. The Standard Model (SM) theory [1] describes these constituents and the relations established between them and three of the four fundamental forces: the strong force, the weak force and the electromagnetic force [1].

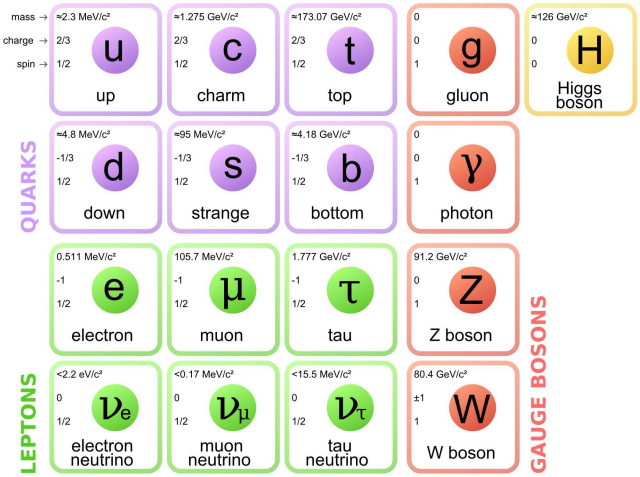

Figure 1.1: The Standard Model (*'Standard Model of Elementary Particles' by MissMJ — Own work by uploader, PBS NOVA, Fermilab, Office of Science, United States Department of Energy, Particle Data Group.*)

According to the SM the elementar particles are split in two families: the fermions (leptons and quarks); and the bosons. There are 12 fermions, 6 leptons and 6 quarks. The Gell-Mann [2] and Weig model description of the quark introduced group theory as a means to describe the behaviour of hadrons, assuming the latter were built from smaller constituents - quarks (q) and anti-quarks ($\bar{q}$). All hadrons found until now carry an integer multiple of the elementary charge of the electron. Additionally they also carry another charge which was called colour and assumes 3 values: red, green and blue.

[1] The gravitational force is the remaining force which does not fit in the SM theory.

As for the bosons they are known as the force carriers. They are the vehicle of discrete energy transfers between elementar particles. There are 5 bosons, each of them associated to one type of fundamental force: the gluon associated to the strong force, the Z and the W bosons both associated to the weak force; the photon associated to the electromagnetic force; and finally the Higgs boson. A controlled lab to study SM theory predictions is, for instance, hadronic collisions.

Collisions such as the ones at the Large Hadron Collider (LHC, CERN), where high energy hadrons collide, are massive producers of coloured quarks and gluons. These elementary particles, constitute the Lagrangian degrees of freedom of the Quantum Chromodynamics (QCD) Theory. QCD then stands as a Quantum Field Theory which studies the strong interaction at experimentally accessible energies. The detection of these high energetic collisions is done in the form of colourless hadrons. These particles are conglomerates of quarks and gluons joined together by the strong force. The interactions are approximately one hundred times stronger than the electromagnetic equivalent, extremely short ranged ($\approx$ 1fm) and with associated energy $\approx$ 1 GeV (mass of the proton).

The QCD Lagrangian can be written as

$$\mathcal{L} = \bar{\Psi} i \not{D} \bar{\Psi} - m \bar{\Psi} \Psi, \tag{1.1}$$

$$\not{D}_\mu = \partial_\mu - i g T^a A^a_\mu. \tag{1.2}$$

It is expressed by quark, $\psi_{\alpha,i,f}(x)$, and antiquark, $\bar{\psi}_{\alpha,i,f}(x)$, fields: Dirac matrices that transform under a non-Abelian SU(3) representation. On the other hand, gluons, $A^\mu_a(x)$ are a result of the QCD colour gauge invariance and appear in the Lagrangian as Lorentz vectors. While quark fields are described by the associated Dirac Spinor, colour index, $i = 1, 2, 3$ (pictorially associated to a colour) and flavour, f, (quantum number which can assume 6 different attributes: top, bottom, charm, strange, up, down), gluons are flavour-blind and do not carry flavour labels. They carry, nonetheless, a colour index $a = 1, ..., 8$.

QCD has two fundamental features: confinement and asymptotic freedom. The first means that only colour singlet particles, that is, particles that transform as singlets in the SU(3) algebra, can survive in a long space-time scale. This implies that hadrons are then the only possible option to find elementary particles under normal conditions of temperature. That is, confinement forbids the manifestation of asymptotic freedom states carrying colour at normal conditions of temperature and density. The remaining feature implies that, at short distances, which necessarily means at high energies, quarks and gluons experience a progressive weakening of the interaction associated to the strong force amongst such particles.

The behaviour of quarks in this state is similar to a quasi-particle state. One can then use perturbative QCD to compute interactions amongst particles. In this regime, the total cross-section production of a final state particles $A + B$ in a proton-proton interaction can be factorized as [3]:

$$\sigma_{pp\to AB} = \int dx_1 f_{i/p}(x_1) \int dx_2 f_{j/p}(x_2) \hat{\sigma}_{ij\to kl}(x_1 p_1, x_2 p_2) D_{A/k}(x_1 p_1) D_{B/l}(x_1 p_2) \tag{1.3}$$

where it is implicit a sum over all the parton types i, j, k, l. The elementary perturbative cross-section is decribed by $\hat{\sigma}$. The outgoing partons kl will follow a parton shower cascade (see section 1.2) and will

eventually hadronize into the final-state particles A and B. This process is described by the fragmentation functions (FFs) $D_{A/k}$ and $D_{B/l}$. Lastly, the hard process cross section also depends on the parton distribution functions (PDFs), f_i and f_j that contain the probability density of a parton carrying a momentum carried x_1 and x_2 of the protons initial momenta.

1.2 Jets and QCD parton showers

Colour coherence problems are common ground to any gauge theory. Partons cannot exist as final-state particles so they will produce other particles in a cascade-like process known as the Parton Shower. This process transfers the original parton energy to multiple lower energy particles and ends with the formation of colourless hadrons. Coherence effects govern the structure of the QCD cascade [4]. A manifestation of coherence of the emissions is the angular ordering [5] of the shower and another consequence is the dead cone effect for heavy quarks [6] [7]. In QED angular ordering can be derived heuristically. Further radiation off the electron or positron is suppressed in certain regions of the phase space. One considers a photon decaying into a pair of e^+e^-. If the angle between the e^+e^-, θ_{ij} is smaller than the angle formed between the emitted photon k and the electron/positron, θ_{ik}, then the emitted photon perceives the electron positron pair as an unresolved charge neutral object and no radiation occurs. Instead, if the emitted photon is emitted with a smaller angle, the electric charge of the individual leptons can be resolved by the photon and radiation takes place. A similar picture can be derived for QCD, with the difference that gluons carry colour charge.

Let us look into this case. The probability of a soft gluon to be emitted by a quark is given by:

$$d\sigma_{Q\to Q+g} = \frac{\alpha_S}{\pi} C_F \frac{\sin\theta d\theta}{1-\cos\theta} \Theta(\cos\theta - \cos\theta_{q\bar{q}}) \tag{1.4}$$

where θ is the emission angle, $\theta_{q\bar{q}}$ the angle between the quarks, C_F the colour factor, ω the energy of the gluon's emission, and α_s the coupling constant. Summing up, in QCD the coherent radiation of soft gluons by an unresolved pair of quarks is no longer zero but the radiation acts as if it were emitted from the parent gluon imagined to be on shell, as illustrated in figure 1.2. This leads to a conservation of an angular-ordered parton shower.

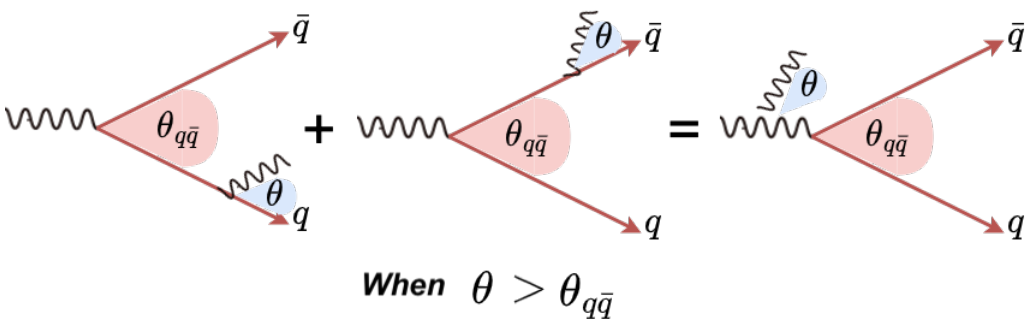

Figure 1.2: Angular ordering for wide angles

Events obtained from a parton/anti-parton interaction are characterized by a chain decay into new pairs of $q\bar{q}$ - the parton-shower (figure 1.3). This process ends when partons bound into final-state hadrons and form a collimated spray of particles called jet. To a very low extent, it is possible to make correspondence of each jet to a quark/gluon that originated it. In fact, jets are defined in [8] as collimated sprays of energetic hadrons, which result from the fragmentation and hadronization of quarks and gluons, such that they are a proxy for the original particles. The fragmentation of these partons can be analysed through the study of the substructure of the jet.

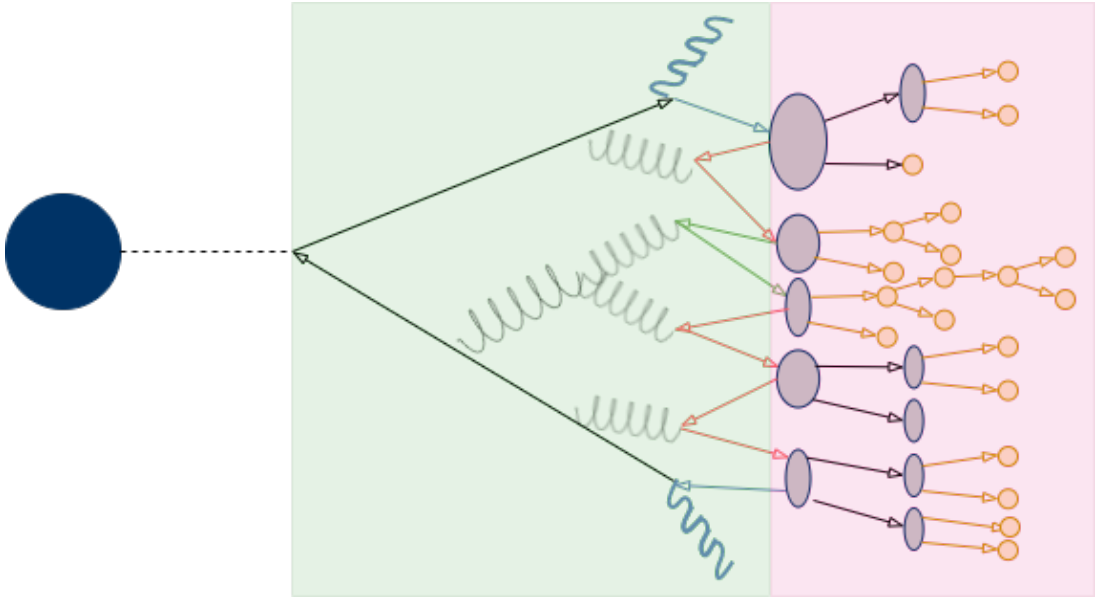

Figure 1.3: Illustration of the final state components of a $q\bar{q}$ production: the parton shower (in the green area) and the hadronization (in the pink area) where hadrons collimate into jets; the energy in the colour flux flux between q and $\bar{q}$ allows to form a new pair $q\bar{q}$ until the partons merge and form hadrons.

As such, jet clustering algorithms are one of the most important analysis tools to study high energetic collisions as they allow to understand QCD mechanisms. A jet clustering is made of a set of rules, which are obeyed by the majority of methods. This guidelines are resumed in [8]: the method must be simple to apply both experimentally and theoretically; it should be defined in every perturbative order; it should contain finite cross sections in all orders of perturbation theory and these cross section should not be affected by hadronization. Among these algorithms, the sequential recombination algorithms are the most widely used. These distinguish themselves by the way they compute the distance, d_{ij},

$$d_{ij} = \min(p_{ti}^{2p}, p_{tj}^{2p}) \frac{\Delta R_{ij}^2}{R^2} \tag{1.5}$$

between particles with transverse momentum (p_T), p_{ti} and p_{tj} [9]. Equation 1.5 includes the R parameter which is responsible for the angular reach of the algorithm and is usually defined as the squared difference between the rapidity (η) and the azimuthal distance (Φ) of the particles,

$$\Delta R_{ij}^2 = (\eta_i - \eta_j)^2 + (\Phi_i - \Phi_j)^2 = \Delta\eta^2 + \Delta\Phi^2 \tag{1.6}$$

The clustering algorithm starts by determining all the d_{ij}'s within a radius of R, pairing particle i to the closest the particle j. Once there are no more particles within the distance R, the method recombines all the particles in a single object - a new jet is formed. The algorithm continues the loop of combining particles in jets until there are no more particles in the event. In equation (1.5) we introduce an exponent parameter, p, which allows to obtain the k_T-like algorithms [10][8][11]. This parameter stands for the power of the energy component relatively to the geometrical one in determining distances. For p=1 we obtain the k_T algorithm, which weights the distances d_{ij} with the QCD emission probability alongside with the relative momentum of particles. The k_T algorithms merge, preferentially, soft particles. By replacing p=-1, one obtains the anti-k_T algorithm [8]. These algorithms tend to merge hard particles in circular areas and are the default algorithms used at colliders. Another special case emerges from the k_T family by setting p=0. The so-called Cambridge Aachen (C/A) algorithm only takes into account the angular positioning of the particles with no weighting in p_T, that is it does not account the momentum of the particles. With the presence of angular ordering, the algorithm is expected to reverse the QCD processes and recover a close approximation of the original particles, and its fragmentation history [11]. For this reason, that it only relies on geometric arguments, C/A algorithms are appropriate to recover the QCD splitting function, that is the energy distribution between partons. Recent studies introduced novel contributions to explore inner jet structure (subtructure). In [10] reclustering procedures are appointed as a new approach to study the jets's substructure.

1.3 Colour flow and hadronization

Jets are colourless objects. Nevertheless they keep information of their colour connections between one another. It accounts for the dependence of the soft gluon radiation on the pre-history. Such relations are not yet completely understood and so experimental analysis is due to occur. Colour connection is a consequence of the SU(3) indices contraction in QCD. The partons separate at high speeds after the initial collision (figure 1.4). The gap between them originates a colour flux with enough energy to produce $q\bar{q}$ pairs.

A chain process is then initiated until quarks pair into jets of colourless hadrons. A single pair is created from a single photon/weak boson/gluon. Additional colour degrees of freedom are also added by radiation [3]. As such the hadronization process occurs at the end of the parton shower, addressed in the previous section. It can be described as a transfer of the QCD colour degrees of freedom resulting from the parton shower to the newly created hadrons. Hadrons are the final particles one can access at the end of high energy collisions: one cannot access the partons at the parton shower due to the fact that they are coloured particles, as we introduced earlier in this chapter. Models are required to suppress as much as possible the limitations in describing the process since calculations are not possible [3]. The two most used models are the Lund-string model [12], which is used in the MC generator PYTHIA [13], and the cluster hadronization model present in SHERPA [14] and HERWIG [15][16].

The coloured link between jets provides a useful superstructure observable. The colour flow will influence the type of hadronization one can obtain [17]: a colour singlet particle, such as the Higgs, which decays into

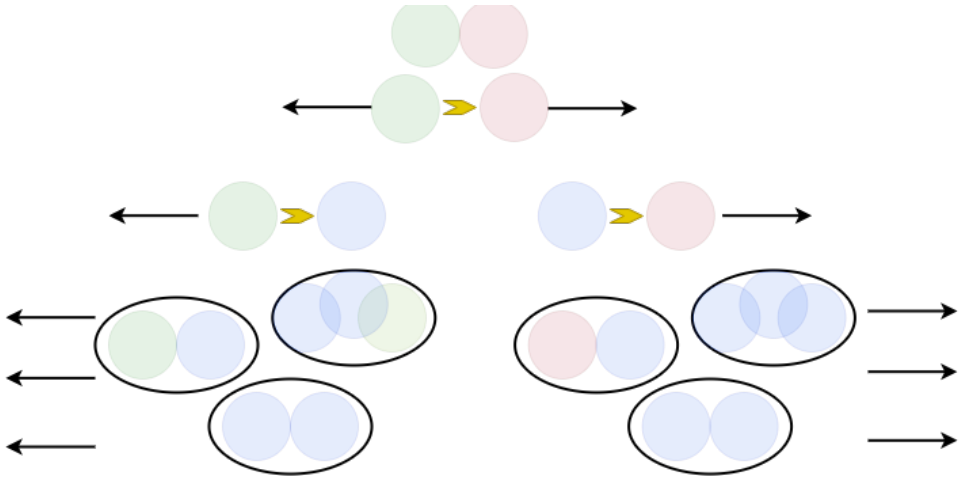

Figure 1.4: Hadronization process and colour flux (yellow arrows): the initial partons starting moving away from each other at high speeds; the colour flux between them has enough energy to form new $q\bar{q}$ pairs; this chain will end when the hadronization occurs

two colour connected partons; or instead a colour octet, a $g \to q\bar{q}$ decay, with two quarks sharing a colour correlation with the initial state parton. The colour flow between jets is physical, leading to the possibility to retrieve information on the colour connections in the event.

1.4 The Quark-Gluon Plasma

A few millionths of a second after the Big Bang, the Universe contained an incredibly dense and hot mixture of constituents, dominated by quarks and gluons. As we have discussed in section 1.2, QCD confinement forces the combination of quarks and gluons into more complex colourless particles: hadrons. This means that one can only obtain this primordial state of matter when asymptotical high temperatures are reached (or, equivalently, at very short distances) and in the presence of a low chemical potential. That way the strong interaction becomes weakly coupled due to the action of asymptotic freedom and one is then able to describe the medium with weak-coupling perturbation theory. Doing so, one obtains at zeroth order of the coupling constant a free plasma of quarks and gluons (QGP) [3][18]. The QGP is characterized as a high temperature matter phase which can be obtained from fundamental gauge theory, and can be described as a fluid. That way one can use phase matter diagrams such as the one in figure 1.5 to describe it.

This state of matter is observed at heavy ultra-relativistic ion collisions. Experiments on QGP are performed at the Relativistic Heavy-Ion Collider (RHIC) and at the Large Hadron Collider (LHC) ([18] and [3], where a review on the results from both colliders is performed). A way to probe QGP is through the jets that were introduced in section 1.2.

Processes associated to heavy ion collisions. which involve large momentum exchanges can be described using perturbative expansions. Such approach is allowed by the QCD assymptotic freedom property. The hard processes described by a perturbative cross section of the type $\sigma(x_1, x_2, Q^2)$ occur in a very narrow time window, $O(1/Q)$ [19]. Now, the study of events like the latter allows to characterise the medium properties since the long distance parts of the expansion are modified when in contact with the medium while the hard

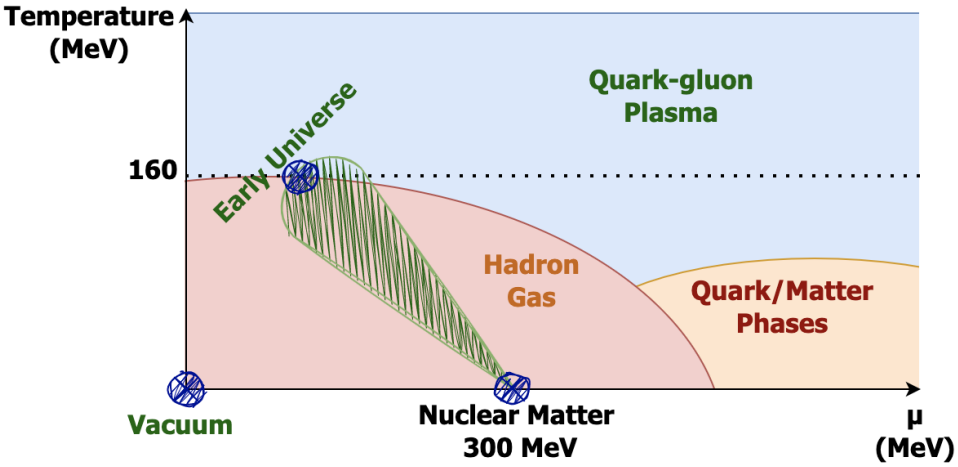

Figure 1.5: QCD phase space: description of the matter phase space in terms of temperature and chemical potential

process remains almost unchanged in nuclear collisions. This is the case of the modification induced by a dense or finite-temperature medium in the evolution of fragmentation functions of high-p_T particles. In these events, a hard jet parton is forced to propagate in a dense QGP formed in heavy ion collisions. During the propagation in the medium, the jet will interact with the thermal partons, which form the QGP. Such interactions cause the loss of energy and a broadening of the transverse momentum distribution. These boosted partons will propagate with matter, radiating gluons while they lose energy. The result of such interaction in the behaviour/structure of jets is jet quenching.

Jets are a very good object of study of the effects of QCD since they are well controlled and defined in the theory for p-p collisions. As we already know, the QGP is characteristic of the early stages of heavy ion collisions. It is natural that in such collisions, due to the presence of QGP medium, that jets propagation suffer changes relatively to the p-p equivalent. The main property associated to these changes is energy loss, that is induced by multiple interactions with the QGP constituents. A cartoon exemplifying this process is shown in figure 1.6 [20][21][22].

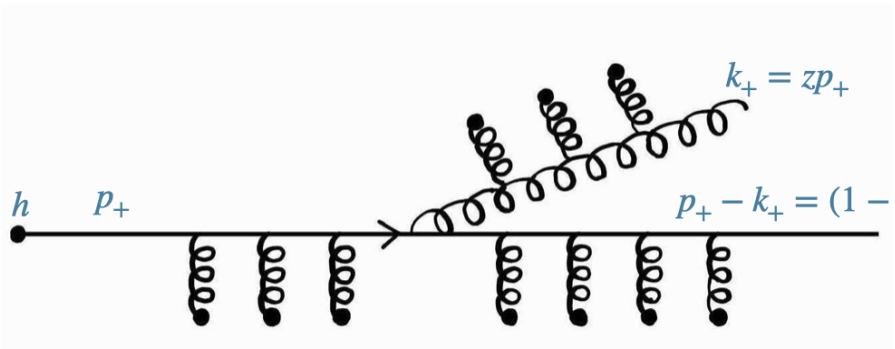

Figure 1.6: Gluon emission, the dominant energy loss process in the propagation of energetic partons

That being said, jet quenching can be perceived as the group of phenomena in hard heavy-ion collisions caused by the interaction of boosted jet partons and the QGP constituents. When in the presence of

medium the properties of jets are altered. On one hand the longitudinal structure of the jet changes, as given by the fragmentation functions. On the other hand, there are also changes in transverse structure: there is an expected broadening of this due to multiple scatterings with the medium [19]. In addition, the expected colour coherence from vacuum showers, as explained in section 1.2 is expected to be broken. This constitutes yet another motivation to use jet pull in an Heavy Ion collision environment, to asses whether the effect is indeed broken.

1.4.1 Colour (De)Coherence

As we mentioned earlier, soft gluons arrising from hard processes are the main responsible for the interference effects. Such effects make it possible to measure explicit non Abelian features of the theory. The effect that the medium induces in jet evolution is still not quite understood. In [23], work was done on studying the quark/anti-quark antenna in a colour singlet. Such set-up offers a useful framework to study intra-jet coherence effects with emphasis to angular ordering. The focus of this work is on the medium induced part of the radiation spectrum off a $q\bar{q}$ in a colour singlet. The results culminate in the conclusion that at the soft limit the interaction with the medium implies a rotation of the pair, inducing emissions at large angles - close to the emissions of an octet antenna in vacuum. To this result they attributed the designation of anti angular ordering.

In addition to the usual angular-ordered emissions, due to the interaction with the medium, gluons can now be emitted at larger angles thus destroying the colour flow that is originated from vacuum jets. We thus expect a clear signal on the jet pull angle. However, HI environment has a background level that might, by itself, spoil the expected coherence from vacuum showers. As such, as the first step, this thesis will test the presence of a HI background into a pp jet (cf. chapter 4).

Chapter 2

Pull Vector analysis in p-p collisions

2.1 Introduction to the Pull Vector Observable

In chapter 1, we saw that jets conserve colour connections among each other. Colour connections provide extra information about the jet in addition to kinematics because it provides an extra observable to complement the information provided by the four-momentum information. Such connections are a graphical picture of the manifestations of the predictions of the QCD theory. In figure 2.1 we may observe on the left the flow of colour associated to colour connected jets, where the final particles share the same colour (pictured in red), and on the right hand side we represent a colour disconnected state.

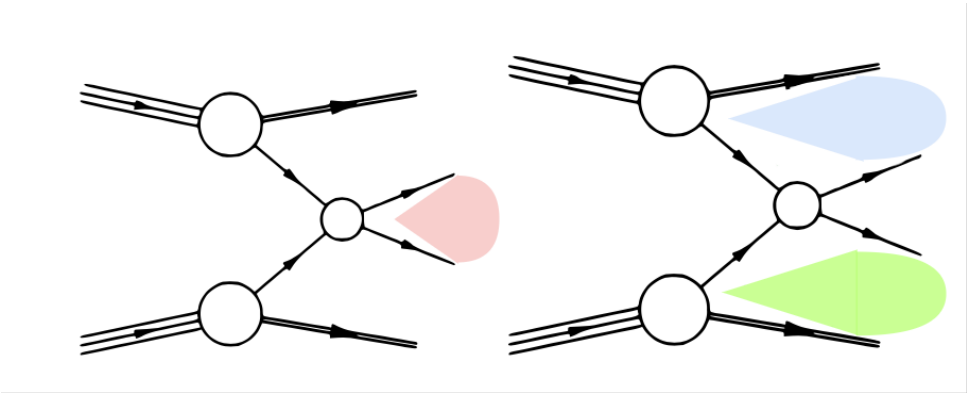

Figure 2.1: The colour connections arrising in the signal and the background.

In [24] the Higgs production, with an associated Z, is studied. The Z association is important so as to ensure that the resulting $b\bar{b}$ pair is not produced at a π angle in the azimuthal plane. With this, they aim to detect the same colour connections that we pictured in figure 2.1. The leading principle is that if such connections should exist, they would be present at hadron level. To achieve it they shower and hadronize multiple times the same parton level configurations of $Zb\bar{b}$ events. Two different cases are compared: the signal which stands for the case where the final $b\bar{b}$ are colour connected to each other and the background where the pair is colour connected to the beam. They manage to retrieve the calorimetric picture of hadronized jets, as shown in figure 2.2.

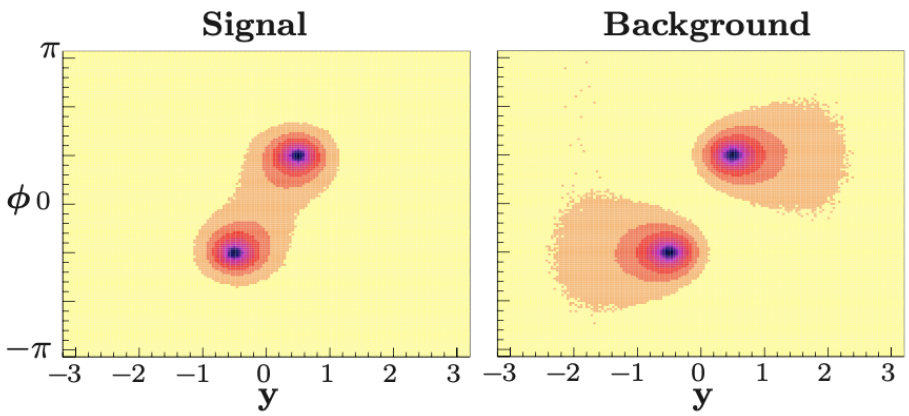

Figure 2.2: The radiation pattern obtained at [24] were we can easily detect the superstructure feature associated to colour connected jets

We can see that there is an evident colour connection amongst jets at the signal studies. The higher incidence of radiation between the 2 b's in the left panel and the opposite occurring for the background case, makes evidence that the superstructure feature we were hunting plays a role at hadron level: the signal jets tend to radiate towards each other, being that way colour connected, and the background jets tend to radiate towards the beam. Since the colour flow is indeed a flux and for that reason, physical, it is measurable. In order to study this flow of colour, they advance a local observable, focusing only on the particles of one jet: the jet pull.

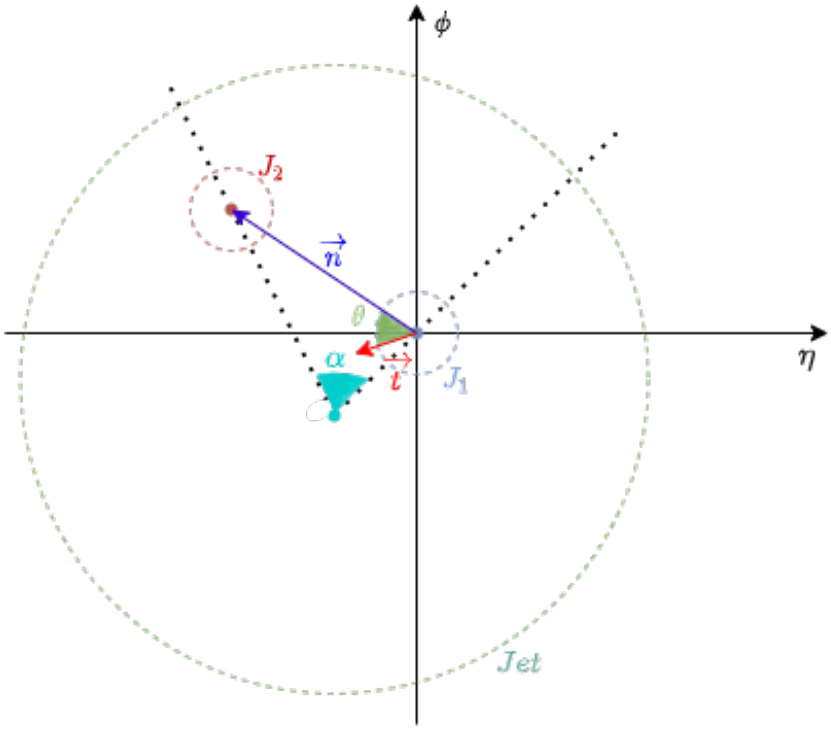

Figure 2.3: Geometric display of the observable; the pull angle is the angle between the pull vector (**t**) and the vector connecting both subjets (**n**).

Let us define the Jet pull vector, $\overrightarrow{t}$, which contains information on the colour flux between two linked subjets [24],

$$\overrightarrow{t} = \sum_{i \epsilon j} |\overrightarrow{\Delta r_i}| \frac{p_T^i}{p_T^j} \tag{2.1}$$

$$|\Delta \overrightarrow{r}_i| = \sqrt{(\eta_J - \eta_i)^2 + (\phi_J - \phi_i)^2} \tag{2.2}$$

where i index is for the subjet constituents and J for the subjets (J_1 and J_2); we also notice that the quantity $\overrightarrow{\Delta r_i}$ stands for the distance in the rapidity coordinate system of each particle to the centre of the leading jet of the event. In figure 2.3, one can get a geometric understanding of the observable. The pull vector is constructed with the information on the jets p_T and each particle's p_T as well. This highlights one of the most important features of the pull vector: when soft particles are involved, their interaction with the surroundings does not affect the behaviour of the pull vector. In other words, the small contribution of p_T provided by such particles would inflict hardly any changes in the pull vector (since it is the sum of all the constituents contribution, the hardest ones will have the highest weight). Since it is a weighted sum of particles' locations, it will point in the direction of the dominant energy flow.

Although the magnitude of the pull vector is also going to be studied, we are mainly interested in the angular distribution (in the rapidity, η, and azimuthal angle, ϕ, coordinate system) of the colour flow , in order to assess whether there is a preferred direction for the latter. We can construct the pull angle, θ , with the information about both subjets. The procedure begins by setting the vector that connects both subjets (easily obtained with the FASTJET [25] variables associated to the object subjet). It is represented in figure (2.3) by the vector $\overrightarrow{n}$.

$$\overrightarrow{n} = \sqrt{(\phi_{J_1} - \phi_{J_2})^2 + (\eta_{J_1} - \eta_{J_2})^2} \tag{2.3}$$

$$\theta = \arccos\left(\frac{\overrightarrow{n} \cdot \overrightarrow{t}}{|\overrightarrow{t}| \cdot |\overrightarrow{n}|}\right) \tag{2.4}$$

Since we obtained the components of the pull vector, $\overrightarrow{t}$, in the previous step, the pull angle, θ, can be computed by straightforward application of trigonometric arguments together with the inner product between $\overrightarrow{t}$ and $\overrightarrow{n}$. This is done in equation (2.4).

One obtains that the pull magnitude is an infrared and collinear safe observable, that is, a modification due to a collinear splitting or the addition of a soft emission would not alter the behaviour of the observable in the presence of a set of hard jets. However, the same does not happen with the pull angle because in the presence of soft emissions the pull angle does not tend to vanish [26]. Studies on the pull angle where also performed in [24]. In Fig.2.4, it is shown the resulting pull angle distribution, named here as $\theta \equiv \Delta\theta_t$ for the same signal and background events shown in Fig.2.2. The left panel refers to take the leading b-jet as reference for the pull vector, $\overrightarrow{t}$, (J1 in Fig.2.3) while the right panel taking the sub-leading b-jet as reference instead (J2 in Fig.2.3). The results obtained were consistent with the behaviour we pointed earlier in this chapter: the signal jets have a tendency to radiate towards each other; because of that, the pull angle distribution peaks at zero while the background distribution does not show a preferred colour flow direction,

that is, the pull angle distribution is uniform. The results are shown in figure 2.4 and allowed to conclude that the pull angle is a good observable to retrieve colour superstructure information.

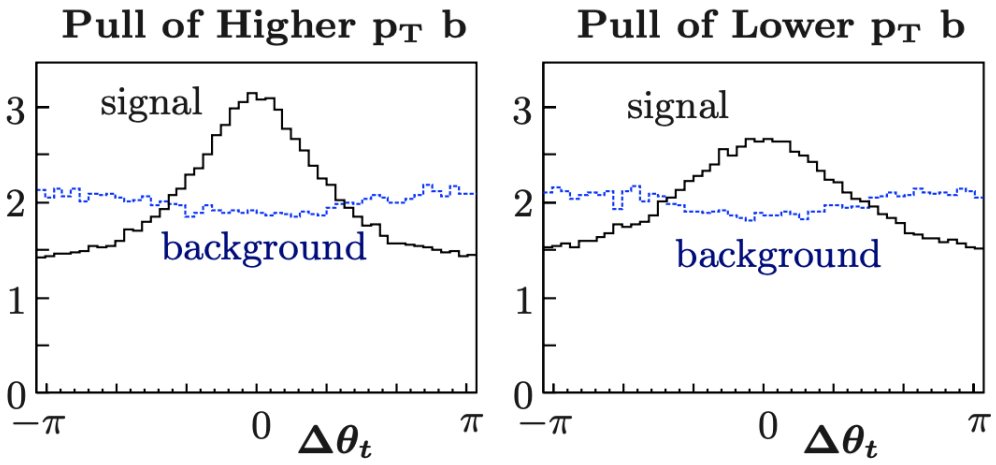

Figure 2.4: Pull angle distributions for the leading (LHS) and subleading (RHS) pull vector; the peak at zero means that as expected the colour singlet pull vector shows a preferred direction [24]

Experimental studies were first addressed by ATLAS experiment [27]. The focus was a di-jet system, using the channel of the semi-leptonic $t\bar{t}$ decay via b-tagging jets, which contains at the same time a singlet and a colour octet which can be defined. As one can see in figure 2.5, the two quarks resulting from the boson (with colour zero) decay are colour connected - singlet - while the b/$\bar{b}$ quarks conserve the colour information from the t ($\bar{t}$ respectively) from which they decayed.

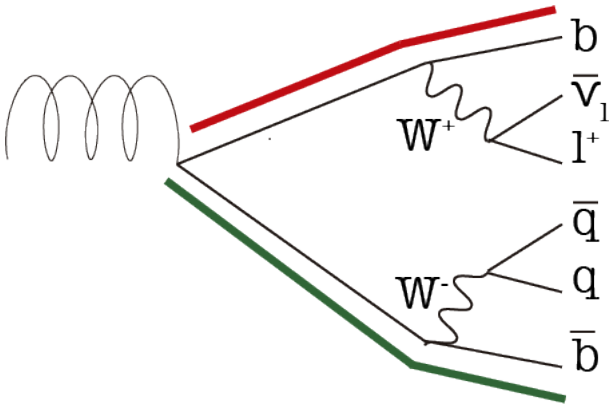

Figure 2.5: Semi-leptonic $t\bar{t}$ decay.

Using this system, the ATLAS collaboration achieved the results in 2.6, where we can see the normalized fiducial differential cross section as a function of the pull angle: on the left panel we see the results for the singlet case while on the right hand side for the octet. The results include several Monte Carlo simulations in coloured markers to compare with the experimental data in black.

By studying several Monte Carlo simulations of pp collisions and comparing them with experimental results from the detector, they obtain results consistent with the theoretical formulations: the singlet distribution of the pull angle peaks at zero and the octet distribution shows a uniform distribution, when comparing with the singlet. The results are promising and helpful to our studies, since they consistently show that the

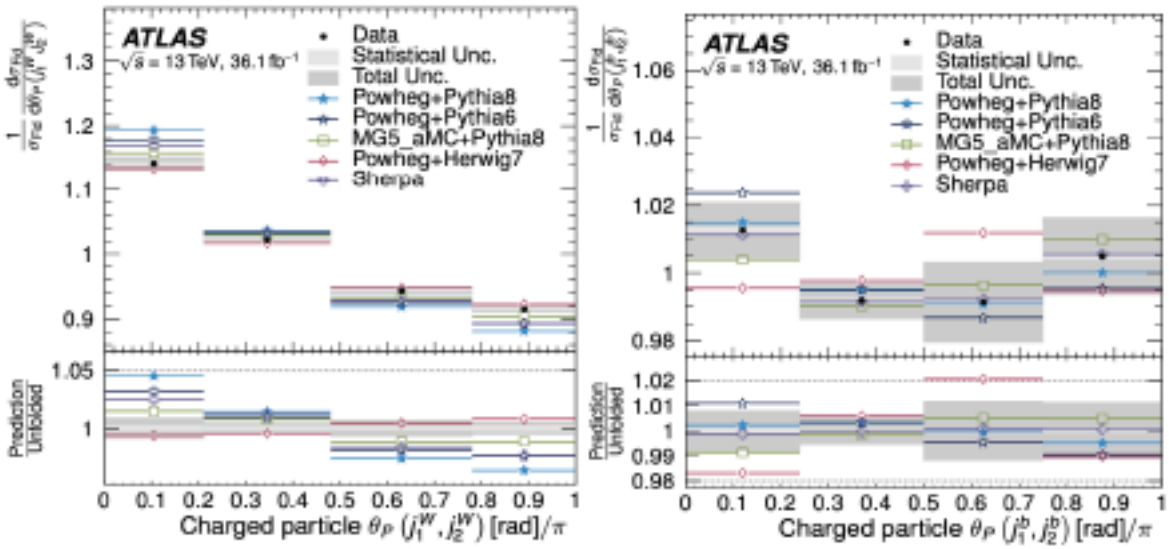

Figure 2.6: ATLAS [27] results for pull angle studies for a singlet and an octet case using a $t\bar{t}$ decay.

superstructure feature we have discussed can indeed be studied from the experiments. We are aiming at studying for the first time a system which can be resilient to a heavy-ion background and also to check if colour coherence is broken. In the next sections we will develop our approach.

2.2 Our Proton-proton baseline in small radius jets

Our goal is to prepare the pathway to heavy ion studies with the pull vector. For doing so, we first introduce the ideal observable to look for colour decoherence in the presence of a QGP. Instead of the ttbar channel, we will need a separate singlet and octet systems, so as to have a sufficiently strong signal to survive in the conditions of our studies. For that we use a double boson weak decay, pictured in figure 2.7 to simulate the singlet case. As for the octet, we require all the hard QCD processes leading to a di-gluon production from the hard scattering.

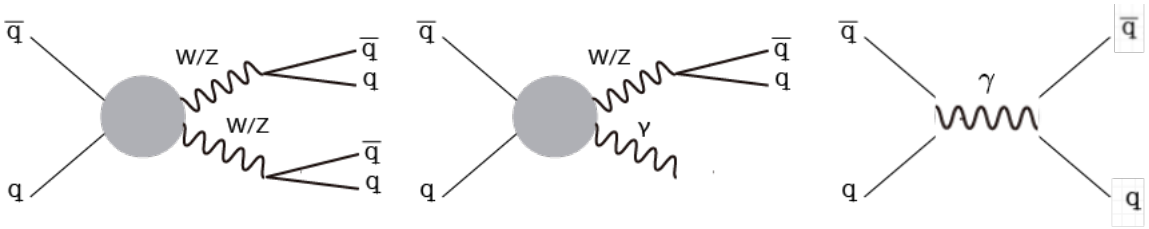

Figure 2.7: Electroweak W/Z decay; the production of gauge bosons supplies a laboratory to study colour singlet coherence effects

Our studies to achieve conclusions on the matter of thermal background influence on the pull vector will be performed step by step. First we establish a baseline in proton proton collisions to assess the regular behaviour of the observable.

2.2.1 Monte Carlo setup and Reconstruction methods

A Monte Carlo (MC) event generator of proton-proton (pp) collisions, PYTHIA 8.2 [28] [13], is used to, separately, produce weighted events of a colour singlet and a colour octet as table 2.1 suggests. This is a tool used to generate high energy parton interactions in pp collisions, going from a few particle interactions to multiparticle phenomena. Among the processes included in the package, it includes the hadronization by using the Lund fragmentation model [29]. In the particular case of the manipulation of the event objects (jets, subjets, particle...) is achieved with the package FASTJET[25].

	Events	
	Singlet	Octet
Channel	Double boson hadronic decay (Z and W bosons)	Gluon splitting
Pythia Channels	**WeakDoubleBoson**:all	**HardQCD**:gg2gg and **HardQCD**:qqbar2gg
Minimum Particle pT	0.5 GeV	
Particle η range	[-3,3]	
Minimum Jet pT	150 GeV	
Mass (J1+J2)	[70,120]	-
Jet Radius	0.2	

Table 2.1: The event definition and the input settings of the Pythia event for both singlet and octet

The experimental cuts we presented are rather important and should be carefully applied, otherwise we could be loosing information. The cuts applied are supposed to approximate our experimental results to the truth distributions, as we are going to approach along this section. One last setting was implemented in the specific case of the singlet events. In order to make sure that the bosons decay hadronically, we use the flag **onMode**[28] for the Z/W and photon.

The pull vector requires, by definition, a two-object system. In the previous section, the system consisted of a subjet system. Now we are about to introduce a di-jet system. In particular case of the singlet, we need to ensure that the jets under study contain the $q\bar{q}$ coming from the boson (Z/W), each jet containing one of the quarks. In the case of the octet we want to ensure that the $q\bar{q}$ pair comes from the splitting of the gluon from the hard scattering. To achieve that, we start by developing an algorithm to pair jets by proximity (in the pseudorapidity frame) and with higher p_T. Our approach uses fully reconstructed jets which in the case of the singlet stand for the $q\bar{q}$ emerging from one boson. One can then merge them in to form a proxy of a "fat jet", which stands for nothing more than the boson. That way, we assume that the two selected jets assume the role of subjets. With this approach we avoid the influence of soft contributions coming from a further cluster sequence and reconstruction looped on the jets constituents. The process is then a direct jet reconstruction without loss of generality, which allows to extrapolate our results for inner jet results.

Although this method allows to retrieve a pair of jets coming, mainly, from the system singlet/octet we expect, many other particles are unrelated to these same systems. It can happen that the jets are paired wrongly and the paired jets are not part of the splitting of the same gluon/boson. For this reason, we also

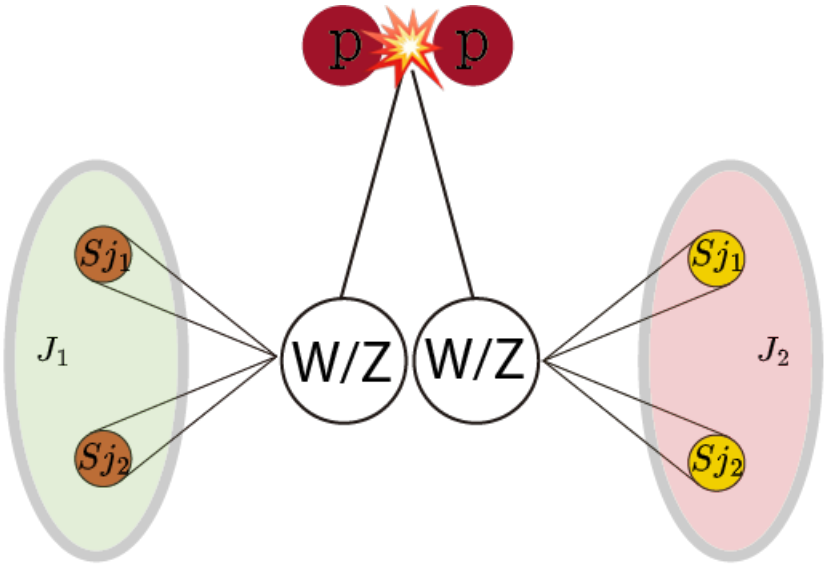

Figure 2.8: Example of the pairing algorithm - Singlet; the algorithm pairs jets first for the distance (Sj_1 and Sj_2) to each other to avoid back to back jets and then by p_t; the sample will be the hardest pair (J_1 or J_2) working the jets in the red/green circles as the leading and subleading "subjet" in the pull angle determination

present the results from an analysis on which we track the history of the particles - *the Monte Carlo truth*. This algorithm is based on a statistical approach. From the event record, we track all the particles from the two out-going partons that are produced in the hard scattering. Once we know the history of all the constituents of both jets, we assume the "parent parton" to be the one that originates at least 60% of the particles within the jet. Next we compare the "parent" of both jets. In case it is the same, the algorithm accepts this event as true MC, otherwise it is discarded. Such analysis is not possible to perform during the experimental process but it is extremely useful to control our methods.

2.2.2 Results on singlet: effect of kinematic and mass cuts

We start by trying to obtain similar results for the settings used in [27] [1]. Which means that we use low p_T jets (minimum p_T of 25 GeV) with a 0.4 radius.

We begin with the correlation between the leading and subleading pull angle. Our benchmark is the correlation in figure 2.9. There we can observe the correlation between the leading (x-axis) and the subleading (y-axis) pull angle. From this we can retrieve that both distribution are completely uncorrelated.

As one can see in figure 2.10a, our sample is also highly uncorrelated. Nevertheless we obtain a non-concentric pattern, unlike the one obtained in ATLAS. In order to come closer to ATLAS' results, we attempt at applying cuts in mass, that is, we restrict a mass window similar to the mass of the Z/W boson - between 70 and 120 GeV (figure 2.10b); and in the fraction of p_T carried by the subleading subjet which we set to be at least 30% of the total p_T of the di-jet system. The p_T cuts revealed to be essential to retrieve the almost symmetrical correlation plot between the leading and subleading pull angle. As one can see from

[1] The low p_T case is further addressed in Appendix A. There we present a full analysis always taking the results in [**atlaas**] and in [30] as a standard.

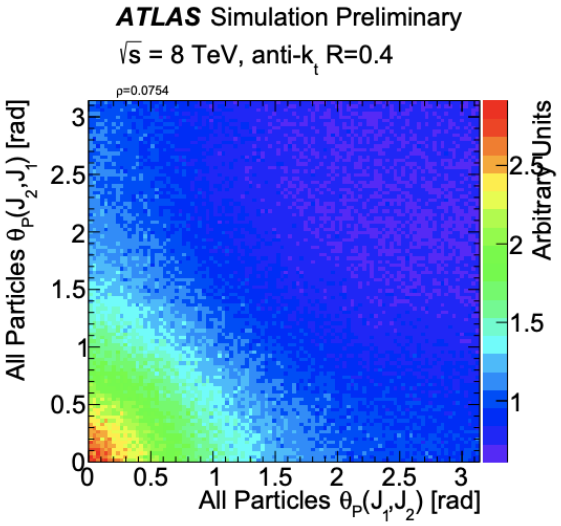

Figure 2.9: Pull angle correlation between the leading and the subleading pull angle [30]

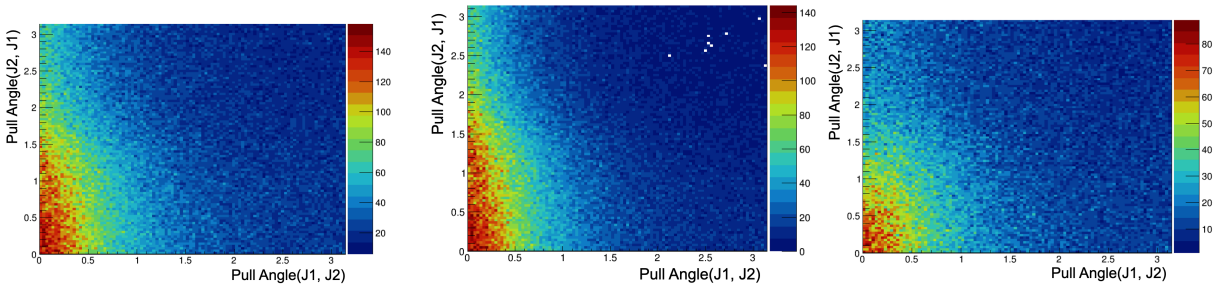

(a) Correlation Pull angle with no kinematic cuts

(b) Correlation Pull angle with cuts 70 <Mass (J1+J2)< 120 GeV

(c) Correlation Pull angle with pT cuts $\frac{pT2}{pT1+pT2} > 0.3$

Figure 2.10: Applying kinematic cuts - The only kinematic cut showing a relevant change to the correlation between the leading and subleading pull angle is the p_T cut; Jet radius 0.4

figure 2.10c, only the introduction of this cut would bring our results closer to the ones obtained in Atlas. That also means we are making the subleading subjet closer in momentum to the leading subjet, reducing then the asymmetry and balancing both jets.

As for the octet system, the mass cut would definitely not be possible to apply. Contrary to what happens regarding the singlet, where we have an expected mass signature, the same does not happens. In the former we are aiming at reconstructing a boson will in the latter the reconstruction relies on a gluon. Therefore one concludes that there was no need to implement any cuts, as one can conclude from the results in the following chapters. There we can prove the closeness of the octet results to the MC truth results.

We now proceed to test the cuts in the settings we are to use throughout our study, that is high-p_T jets with 0.2 radius. We use these settings due to the nature of our singlet system. In the following discussion we will present the results for pp collisions at these p_T conditions for both singlet and octet (a further analysis targeting the $c\bar{c}$ case is done in Chapter 3) and the comparison of these experimental results with the truth distributions. We will discuss in section 3 other methods including the analysis of the pull vector for subjets reclustering methods.

In figure 2.11 a comparative study of the pull angle with kinematic cuts, without and the MC truth

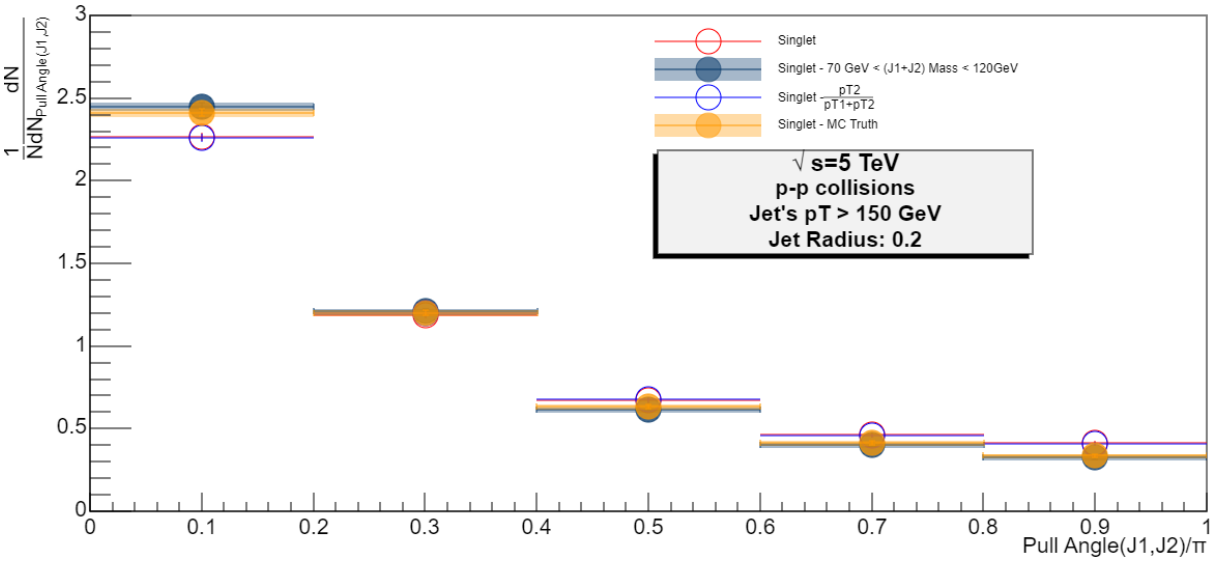

Figure 2.11: Pull angle(J1,J2) distributions with the comparison of the cuts 70 < Mass (J1+J2) < 120 GeV and $\frac{pT_2}{pT_1+pT_2} > 0.3$ with the hadron level MC truth and with no cuts applied

distribution is performed. We can see that the pull angle distribution is equivalent to the MC truth distribution when comparing to the cut in mass. To confirm such claims we present the deltaR distribution in the same conditions in 2.12. It is visible from the latter that the cut in mass(J1+J2) implies that we are focusing on the closest prongs, which should be the expected behaviour since we are dealing with high-p_T jets. This means the resulting decay from the double boson system will be collimated to the collision centre.

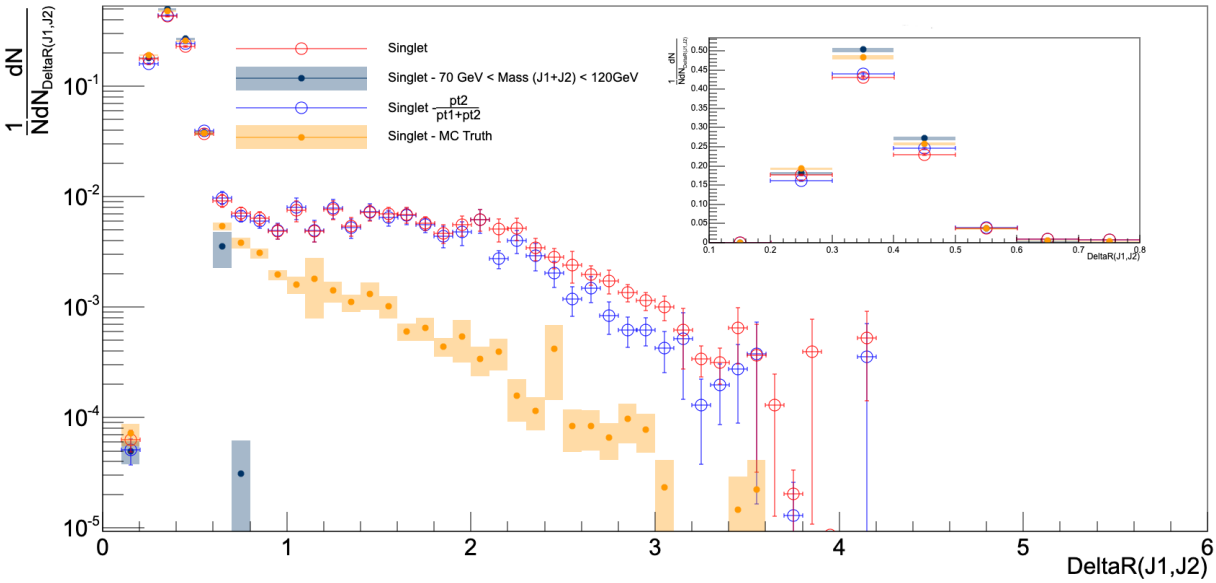

Figure 2.12: DeltaR(J1,J2) with the comparison of the cuts 70 < Mass (J1+J2) < 120 GeV and $\frac{pT_2}{pT_1+pT_2} > 0.3$ with the hadron level MC truth and with no cuts applied

That being said one can see from the results presented until now that the p_T restriction does not inflict hardly any changes to the system, neither it makes its behaviour closer to the MC truth distributions. Only the mass cut provides a major role in obtaining a close enough system to the MC truth distributions for the singlet system.

2.2.3 Results on singlet and octet: effect of centre-of-mass energy

We start our discussion on the baseline results by introducing the Pull Angle results for $\sqrt{s} = 13TeV$ and $\sqrt{s} = 5TeV$ for jets with a minimum p_T of 150 GeV (an extended discussion for low-p_T jets is performed in Appendix A).

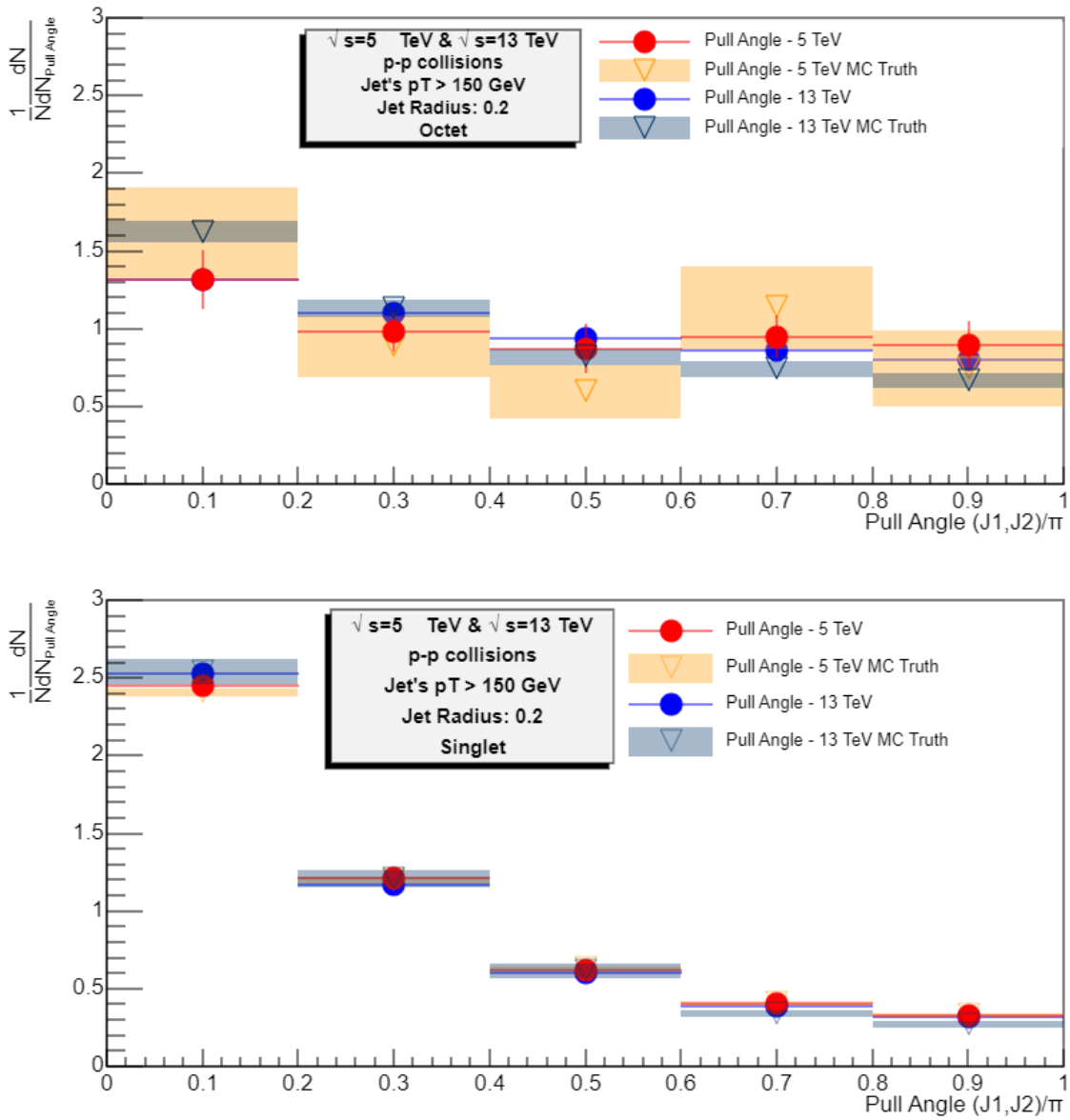

Figure 2.13: Pull angle distribution for the leading subjet for the singlet and for the octet. From this plot we understand that the centre of mass energy does not play a relevant role for our results, so we can maintain the 5 TeV value as standard for the analysis.

In figure 2.13 we start comparing the pull angle distributions for both 5 TeV and 13TeV and comparing the reconstructed case with the MC truth distributions. The truth distribution was obtained by studying the history of the leading and subleading jets' particles. We trace the history of all the jets particles until we reach the $q/\bar{q}$ coming from the hard scattering. We assess the momentum influence that each initial parton as in the jet. If both jets are mostly influenced by the same parton we accept the event as the MC truth.

We understand that, as expected, one obtains similar distributions for the 2 values of centre of mass energy. The singlet presents a peaked distribution at pull angle $\theta = 0$, as expected. This means that we are in the presence of a pair of connected jets. On the other hand, the distribution for the octet presents a flat shape. One can also notice a big difference between both signals, which means that our singlet and octet are well differentiated by this observable. That being said in the following discussion we will proceed with $\sqrt{s} = 5$ TeV, which is similar to the value used by the Atlas experiment.

One can also observe that the cuts in place are fulfilling their purpose. In the particular case of the singlet, the similarity in pull angle distributions with the mass cut and MC truth shows that our kinematic cuts are putting our setting's results close to the true double boson system decay. As for the octet, the insignificant differences are most certainly explained by the fact that we did not apply kinematic cuts to the distributions. The fact that such differences are not significant is another proof that our octet does not require any kinematic cuts to get close to the MC truth distributions.

It is also presented the pull angle correlation for leading and subleading pull angle, by plotting the leading pull angle (x-axis) versus the subleading pull angle (y-axis): in figure 2.14b we obtain the expected almost symmetric distribution. We also introduce the pull angle correlation in the case of the octet, for a matter of comparison in figure 2.14a. As expected there is no preferred direction or symmetry in the correlation, since that comes from the construction of the pull angle for a disconnected system such as the octet.

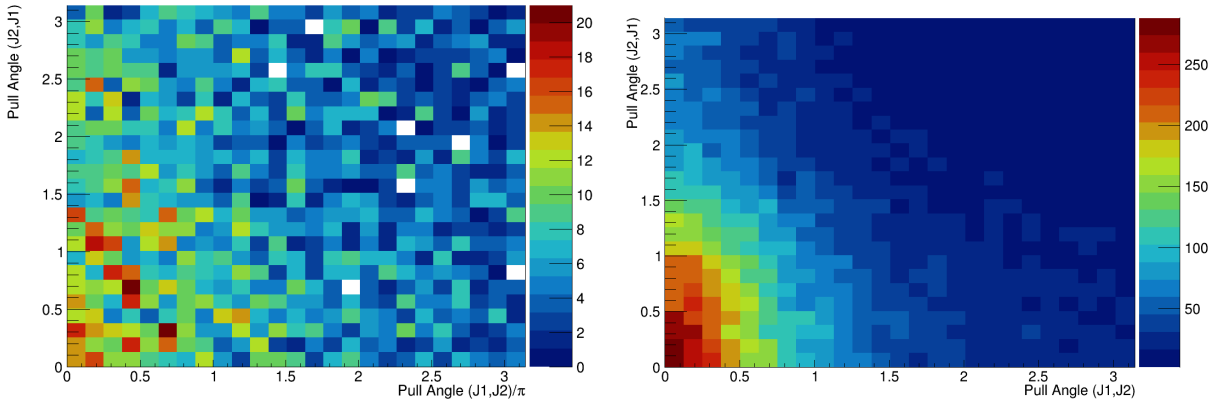

(a) Pull Angle correlation for the octet. The distribution appears as expected not to show any preferred direction or correlation at all between both variables

(b) Correlation of leading and subleading pull angle with mass cuts $70 < MassJ1 + J2 < 120$ GeV. This distribution shows a slightly asymmetric tendency.

Figure 2.14: Singlet and octet correlation of leading and subleading pull angle for radius 0.2, One can see that for the octet we have a diffuse distribution, as for the singlet by applying the cuts we retrieve the almost symmetric distribution observed in ATLAS

On the pull magnitude, we perform in figure 2.15 the same comparisons we did for the pull angle (centre of mass with the reconstructed and the MC truth for both the singlet and the octet). One can retain that the magnitude of the vector is consistent for both singlet and octet. We can even say that the kinematic cuts in mass allowed to obtain a closer behaviour to the truth distributions at $\sqrt{s} = 5$ TeV.

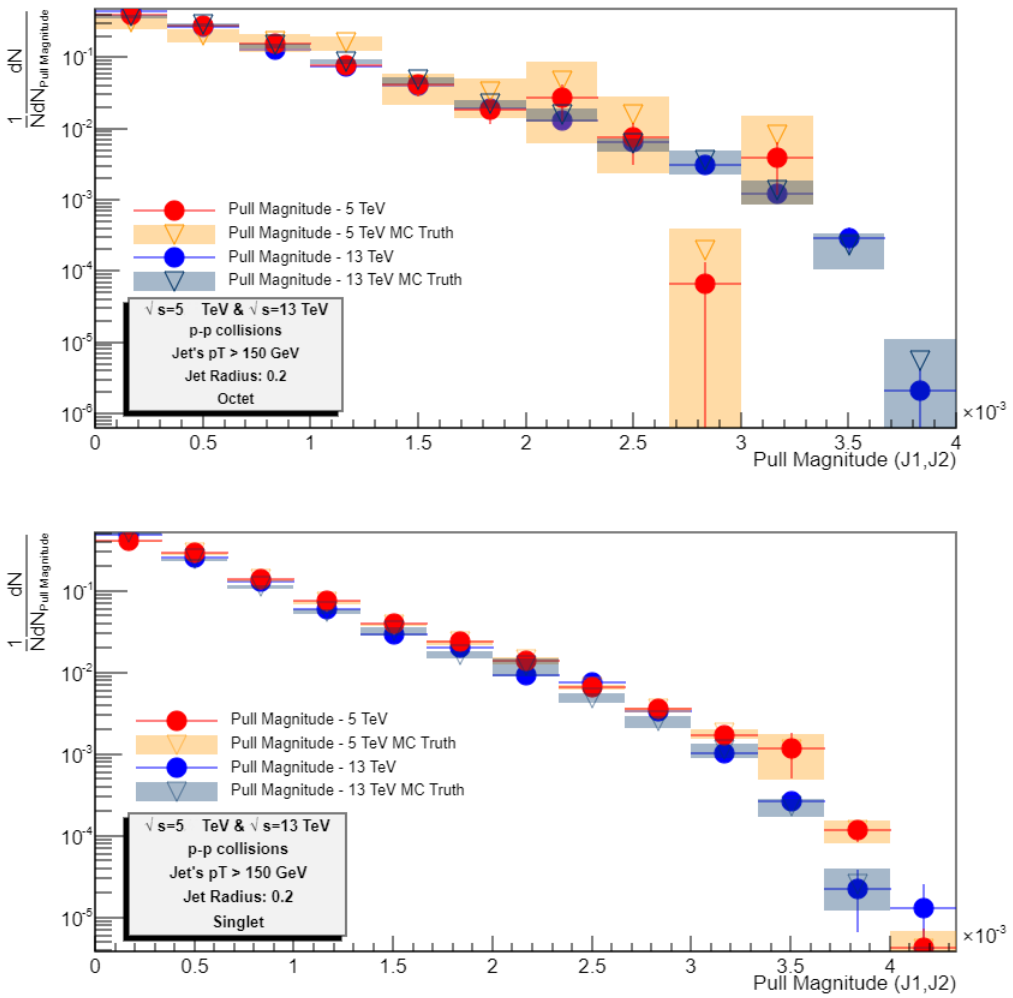

Figure 2.15: Pull magnitude for singlet and octet. Comparison between truth and post-cuts distributions allows to re-ensure our previous statements.

That way, we can now proceed to a first comparison of octet and singlet since we already have a well defined system and observable.

We are now in a position where we can confront the results we obtained for both the singlet and octet at pp collisions. These will then serve as a baseline to the future signals we may introduce during our studies. First, we look into the pull angle in figure 2.16, were we put for the first time singlet and octet in direct comparison. This observable is the one expected to show a greater difference in terms of behaviour due to nature of the two systems under study.

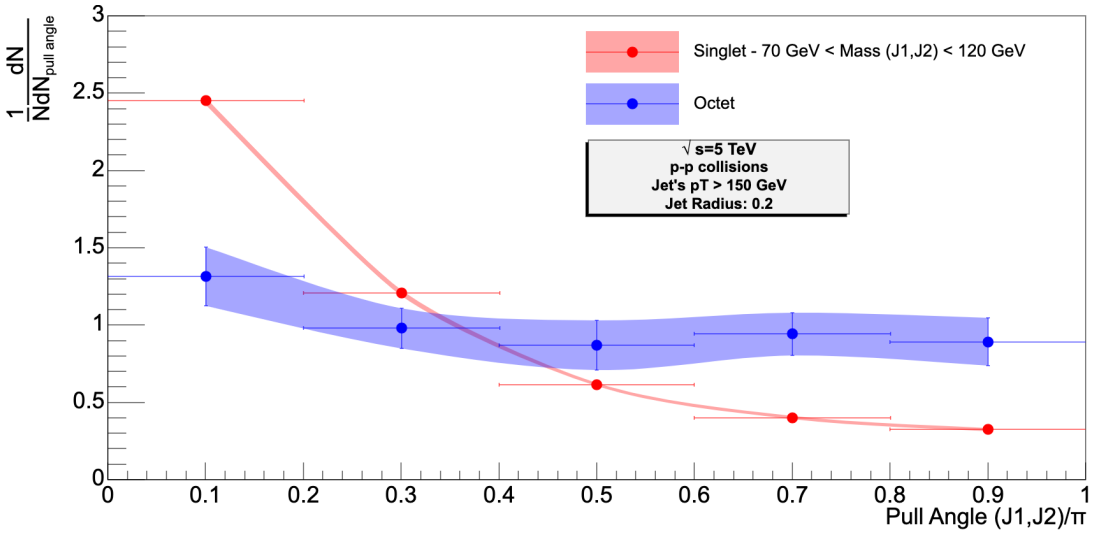

Figure 2.16: Baseline results for singlet and octet pull angle. One can see that as expected there is a sharp peak for pull angle zero and a much flatter distribution for the octet distribution. That way it is easy to distinguish between both signals

As expected, the signal regarding the singlet shows an evident peak at zero. The difference between the colour singlet and colour octet is also very clear, setting the tone to our next discussions in the presence of a thermal background.

We also present in figure 2.17 the comparison between pull magnitude for both singlet and octet. As predicted there is no major difference between both distributions.

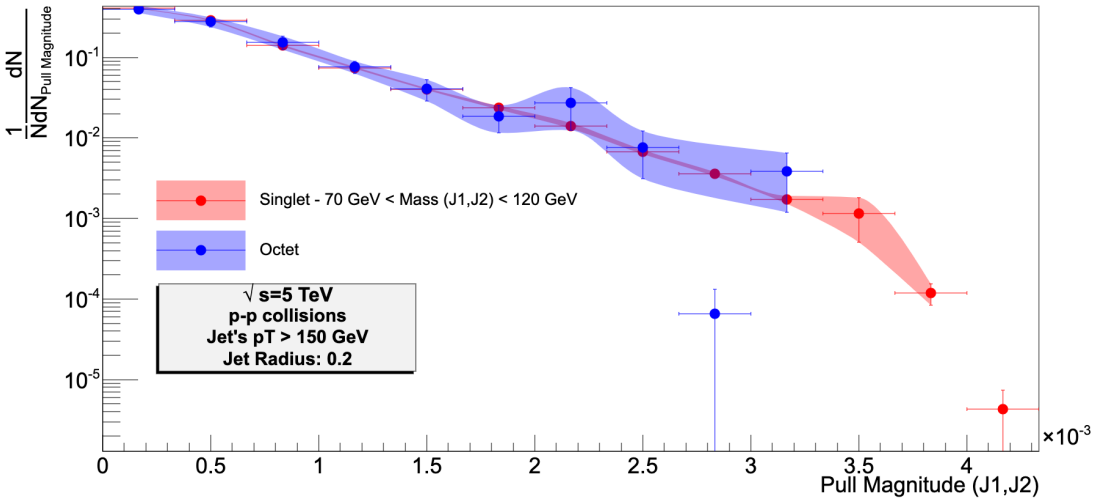

Figure 2.17: Baseline results for singlet and octet pull magnitude. One can see that as expected there is correspondence between both distributions

2.3 Our Proton-proton baseline with jet substructure

Previously, we introduced a method where we only use fully reconstructed jets. We could observe that the results were consistent with the ones obtained at [27]: the singlet signal was distinct from the octet; while the first observed a clear peak at pull angle zero, the second pointed to a uniform distribution.

For completeness of our discussion we also tested the effects of applying the pull vector to reclustered subjets in two different approaches for the same singlet and octet channels.

2.3.1 Soft Drop Grooming

The first approach, consisted on implementing a cluster sequence with an anti-k_T algorithm, applied to the list of final state particles generated by PYTHIA. This allows to obtain jets with a perfect conic shape. We considered R=1 jets with a minimum p_T of 1 TeV, in a range of [-1.5,1.5] in the pseudorapidity plane and a particle $p_T > 0.5$. The next step consists on a reclustering sequence where we use, as mentioned in the previous section, a C/A algorithm to re-write the jet history. Forcing the final stage of the clustering process to reverse, the declustering process, we obtain two subjets from the parent jet which we order by transverse momentum (p_t) magnitude (let J1 be the leading - hardest/higher p_t - subjet and J2 the subleading subjet). That way we are unveiling the history of the clustering process

At this stage we introduce a grooming method: Soft Drop grooming (SD)[31]. It aims to eliminate the soft emissions (i.e. with a low-p_t) at high angles. By applying it, it is possible to select the hardest/boosted emissions during the declustering process, which are the objects of study of this work. If the subjets pass the soft drop condition,

$$z_g = \frac{min(pt_1, pt_2)}{pt_1 + pt_2} > 0.1, \tag{2.5}$$

where z_g is the threshold cut in the subjet pt and 0.1 is the value that z_g must overcome to be considered, the hardest subjet becomes the parent jet in the following unclustering step, and is then split into two subjets. The iterative unclustering process continues until the hardest branch of the jet can still be split in 2 subjets, or the soft drop criteria is met.

2.3.2 Fully Reclustered Subjets

As an alternative approach, we replace the SD grooming and the Cambridge/Aachen (C/A) reclustering sequence. That way we perform a cluster sequence with an anti-k_T algorithm to the final state particles. We set the jet radius at $R = 1$ and the minimum p_T at 300 GeV. Next we target the hardest jet and perform a reclustering sequence with an anti-k_T algorithm to the jet's constituents. That way we can obtain the 2 hardest subjets within the jet. These subjets are required to have $R = 0.2$ and to be within a range of 1.5 in the η-plane to the initial collision.

2.3.3 Comparison between the jet substructure reconstruction methods

The pull vector provides a distinct angular signature in the presence of a colour singlet and another in the presence of a colour octet: the former results in a peaked representation at pull angle zero which means there is a colour connection between the two prongs; the latter results in a flat/uniform distribution showing that there is no preferred direction to this vector. These ideas helped in the task of choosing the best reconstruction method from the previous ones.

As for the SD grooming method, we present in figure 2.18 the pull angle and deltaR distributions. We may see that the deltaR distributions (figure2.18a) are quite close to the MC truth distributions. However, one may also observe a clear peak at $\pi/2$ for the pull angle in the octet channel as one can see, accompanied with the great closeness between both signals, making them almost indistinct.

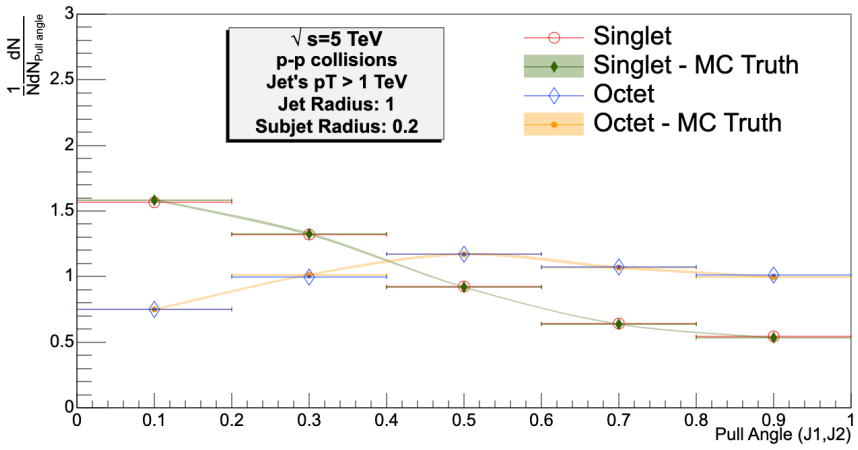

(a) Pull angle distribution for the SD grooming. There is a clear peak at $pi/2$ which is not compatible with the expected behaviour, a flat distribution showing no preferred direction to the pull angle

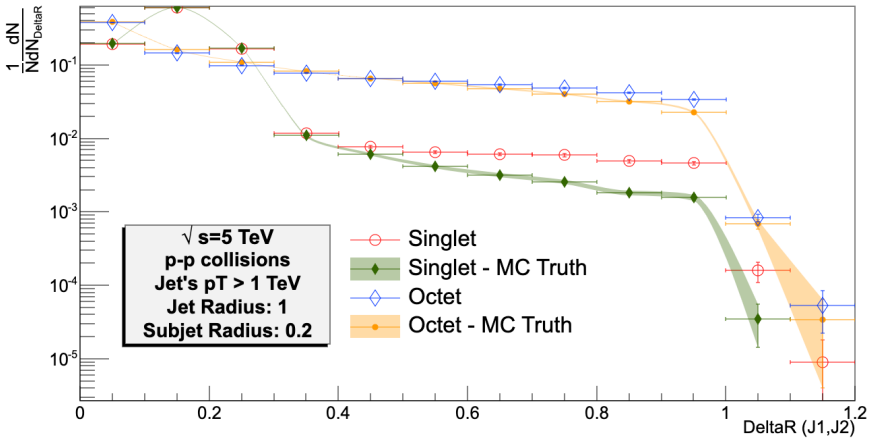

(b) DeltaR Distribution for the octet and singlet for both reconstructed and MC truth distributions

Figure 2.18: Distributions for the SD grooming method

This was not consistent either with our own results presented in section 2.2.3 and the results in [27]

As for the fully reconstructed subjets method, we present in 2.19 the pull angle and deltaR distributions for both the reconstructed case and the MC truth (obtained using the same method as explained previously). From those, one can understand that the method fails in several aspects. Firstly, a note regarding the MC truth distribution for the singlet. There was not enough statistics to present this distribution. That is explained by figure 2.19b, were we show the deltaR distribution again for both cases, reconstructed and MC truth. There we see that the subjets we are positioned back-to-back, with a distancing around π. One expected a deltaR close to the radius of the subjets. That means we are not targeting the $q\bar{q}$ pair we aimed and that we are not reconstructing the boson.

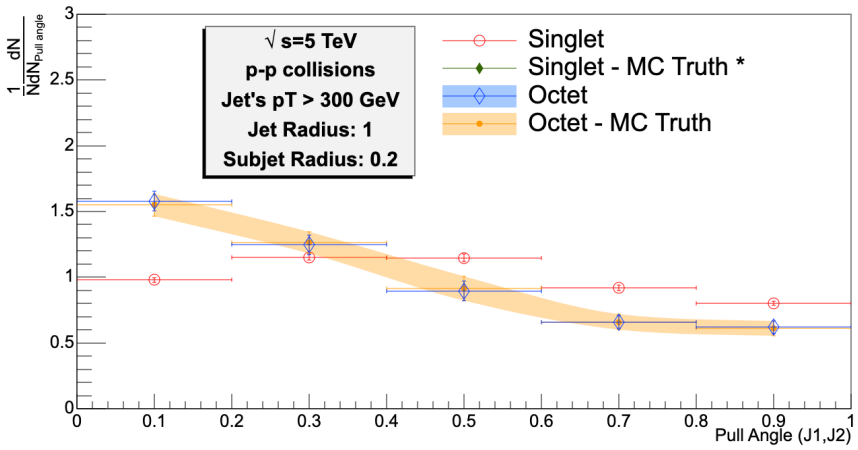

(a) Pull angle distribution for the fully reconstructed subjets.

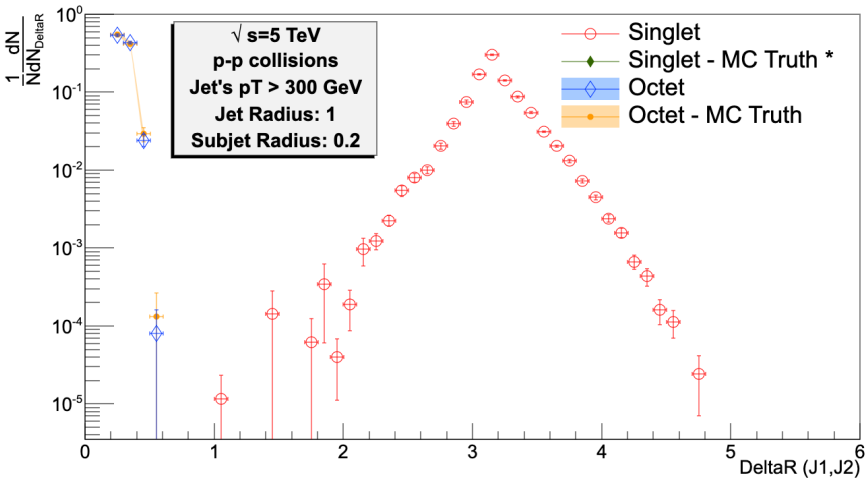

(b) DeltaR Distribution for the octet and singlet for both reconstructed and MC truth distributions

Figure 2.19: Distributions for the fully reconstructed method

Other argument against this method is the correlation between the pull angle for the leading and the subleading subjet. One would expect to find a similar behaviour as found in [27]: both angles should have no correlation. The problem with this as one can see in figure 2.20 is that there is no symmetry between both jets, which is observed in ATLAS' results.

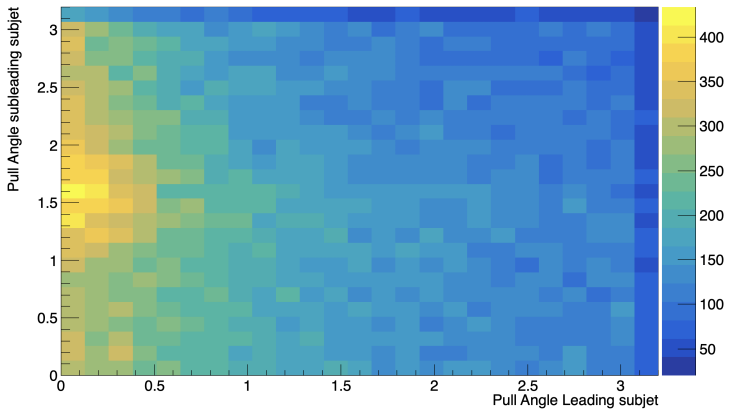

Figure 2.20: The correlation between the pull angle for the subleading and the leading jets is not compatible with the matching plot from [27]

That being said we opted to proceed the following analysis recurring to the jet pairing method, due to the consistency of results.

Chapter 3

The Pull Vector in pp collisions: the $c\bar{c}$ case

The pull vector and, in particular, the pull angle have a typical behaviour in the presence of an octet system: the distribution tends to be uniform for all angular directions. This is confirmed by the results discussed in chapter 2.1 and also by the results obtained by the ATLAS collaboration in [24] for the octet system (where the octet was understood as the background to the singlet signal). We showed the methods we developed to make sure we are targeting jets resulting from the gluon splitting. Nevertheless, there is the possibility that part of our sample for the octet case could come from unrelated systems. By tagging c and b quarks, which are heavy quarks, one has an experimental upper hand when comparing with the QCD jets studied in the previous chapter on the studies of a colour octet. In addition to this the fact that we have a better and easier tagging of the system, makes this a better framework to test our ideas of jet decoherence for a heavy-ion setup (see chapter 1). It is always useful to reinforce that our ultimate goal is to assess the effect that in-medium jet propagation plays in the behaviour of our observables. Hard probes are used, as we also saw in previous chapters, due to the modifications in long distance parts of the fragmentation pattern. These changes will allow a further study of the properties of the medium. Jet decoherence is a phenomenon of in-medium jet propagation. As such, having an octet case that can serve as a benchmark to understand if the jets decohere in the presence of a QGP is important to the extent that only this setup can give us an accurate baseline: since we are looking inside the jet constituents through the study of subjets, we are coming closer to the studies at HI where jet decoherence is studied within jet substructure (subjets) or via nearby small-R jets.

So as to achieve it and for completeness of this document, we aim at narrow the octet system to one we can control at hadron level: D-mesons coming from a $c\bar{c}$ gluon splitting.

3.1 Reconstruction methods

We aim at selecting jets containing D-mesons. These are the lightest charmed mesons, that is, are the lightest mesons containing a c-quark in its constitution and for this reason they are also the most abundantly produced - it is always easier to produce light particles. Each of the quarks of $c\bar{c}$ hadronizes with one light (anti-)quark into a D meson. Our aim is to collect events on which we can pair the two D-mesons coming from the same gluon splitting. Since this is a particular case of the octet used in chapter 2, we will use the same base PYTHIA event settings as in table 3.1, where we can find the list of settings used to produce our results as well as the cuts inflicted to the event particles. In the referred chapter we did not put any restriction to the type of quark decaying from the gluon. Now we are only interested in the events on which the gluon splits into a $c\bar{c}$.

	Events
	Octet - $c\bar{c}$
Channel	Gluon splitting
Pythia Channels	**HardQCD**:gg2gg and **HardQCD**:qqbar2gg
Minimum Particle pT	0.5 GeV
Particle's η range	[-3,3]
Particle's ϕ range	[-π,π]

Table 3.1: The event definition and the input settings of the Pythia event for the $c\bar{c}$ case for 2 fully reclustered jets

Furthermore, since our target is to get D-mesons, we ought to forbid them from decaying. So, to ensure that during the hadronization process the D-meson does not decay into other particles, we use the PYTHIA flag

$$mayDecay = off \quad , \tag{3.1}$$

which blocks the decay of the referred particle. As such, we will select all the possible D-mesons identifying them with the PYTHIA particle code as shown in table 3.2. Moreover, to tag the anti-particle as well, we use the absolute value of the PYTHIA particle code.

D-Meson	Constituents	Particle code
D^+/D^-	$c\bar{d}$	411
D^0	$c\bar{u}$	421
$D^*(2010)$ $(^+/^-)$	$c\bar{d}$	413
$D^*(2007)$ $(^+/^-)$	$c\bar{u}$	423

Table 3.2: D-mesons present in the event

Due to the small gluon splitting rate into $c\bar{c}$ pairs (about 3.5%, [32]), approximately 96.6% of the weighted events do not contain any D-meson. As for the remaining 3.4%, most of them only contain a single D-meson inside the (p_T, η, ϕ) range that we consider (table 3.1). We present this records in figure 3.1a. We can already see that, when present in the event, the most common case is one D-meson per event,

which does not fulfil our objectives. Additionally we also present the p_T spectrum of the D-mesons present in events with the settings described above as well as their spatial distribution in η.

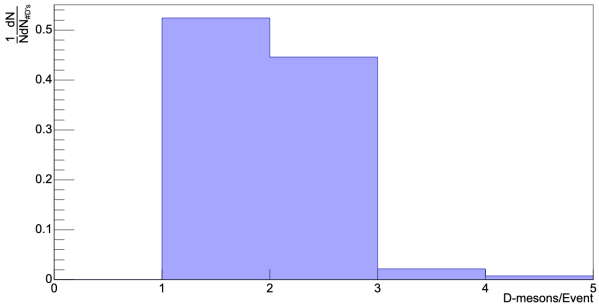

(a) Number of D mesons per event

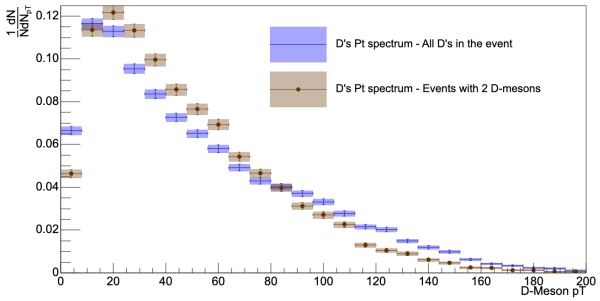

(b) Pt spectrum of the D-meson present in the events

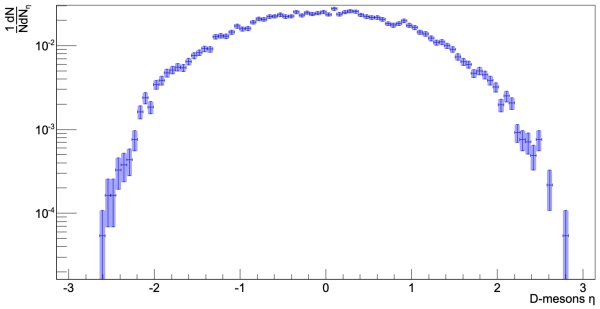

(c) η distribution of the D-meson present in the events

Figure 3.1: D-mesons accessible in the events with at least one of this mesons and with the settings in table 3.1

That being said to the restrictions presented above we need to add another restrictive step: the event must have at least two D-mesons. The two leading mesons of the event will, most likely ,be the ones we will tag during our analysis. As such, it is useful to understand its proximity. We present the deltaR distribution of the two hardest D-mesons in events with at least this number of such particles in figure 3.2a. We observe that the majority of D-meson pairs have a distance between particles close to the jet radius. However we still see a less dominant incidence of events where the pair constituents have a distance close to π which makes them back to back. Comparing this distribution with the difference in η (figure 3.2c) and ϕ (figure 3.2b) for the same 2 leading D-mesons (please recall chapter 1, and the deltaR definition), we can see that the contribution at π in deltaR is given to the particles further away from the beam in the ϕ-direction. We will make comparisons between these results and the results we will obtain along the chapter.

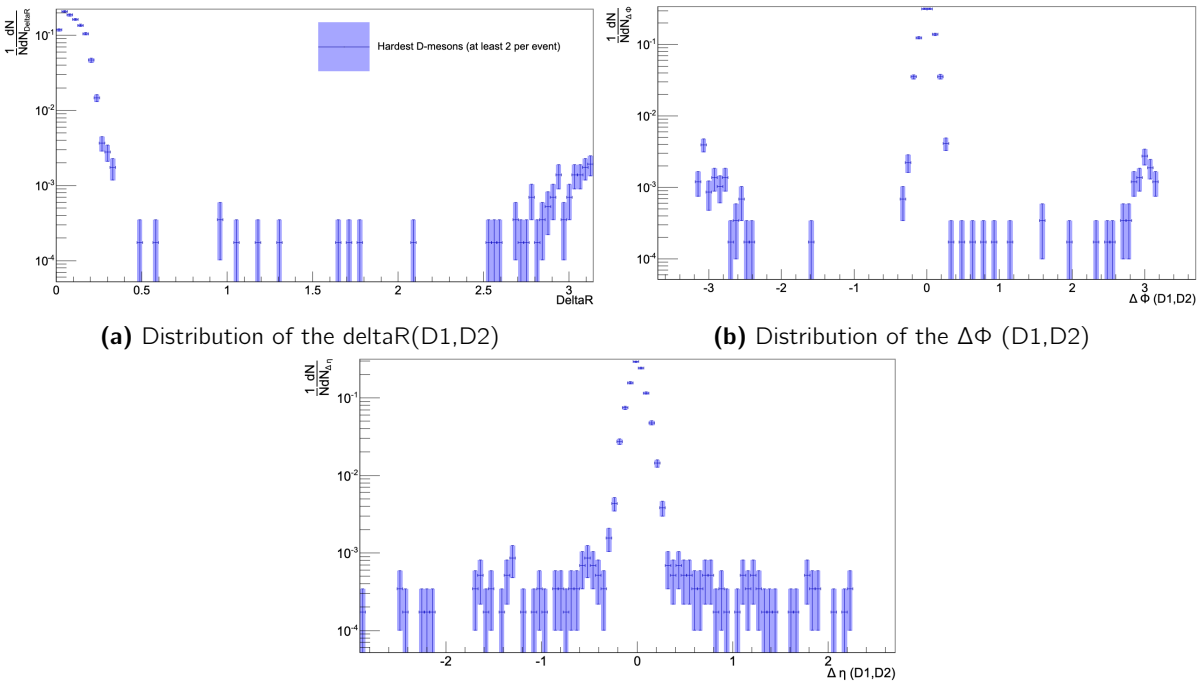

(a) Distribution of the deltaR(D1,D2)

(b) Distribution of the ΔΦ (D1,D2)

(c) Distribution of the $\Delta\eta$ (D1,D2)

Figure 3.2: D-mesons positioning for events with #D-meson>1 tagging, where D1 is the hardest D-meson and D2 the second hardest.

3.1.1 Fully Reconstructed jets

Let us first follow the strategy used to obtain the main results in chapter 2.2.3, that is, pairing fully reclustered jets.

	Events
	Octet - $c\bar{c}$
Reclustering	anti-k_T method
Minimum Jet p_T	150 GeV
Jets' Radius	0.2
Jets' η range	[-2.5,2.5]
Jets' ϕ range	[$-\pi$,π]

Table 3.3: Jet reconstruction settings for the events with described in 3.1

For the PYTHIA settings described in table 3.1, we apply the restrictions in table 3.3 we use an anti-k_T method to reconstruct jets with radius $R = 0.2$. We obtain the number of jets per event as follows in figure 3.3a The figure shows that the majority of the events are not fit for our analysis: recall that we need two jets in order to proceed with the pull vector analysis. One can observe that the most of the collected events have one or no jet at all, within the p_T selection (table 3.3). That being said, our sample will include only the events with two jets. However, we still need to add a new layer of restriction because we need to ensure that each of the jets under study have at least one D amongst its constituents. As for the events with one or more jets, we show the number of jets containing at least one D-meson in figure 3.3b.

The last statement left us with even less available events which are the ones with two jets containing at least one D-meson each as one can confirm from figure 3.3b where we see that the number of events

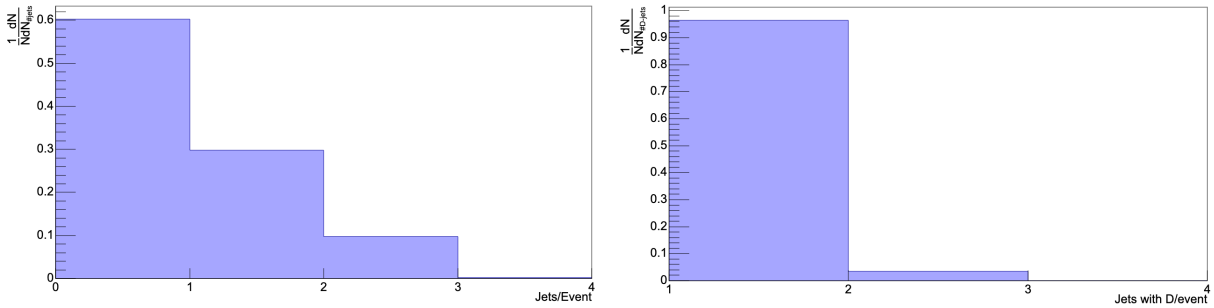

(a) Number of jets per event **(b)** Number of jets with at least 1 D-meson per event

Figure 3.3

with two jets which contain at least one D-meson is relatively small comparing to events with only one jet in such conditions. In table 3.4 it is listed the efficiency of each of the reconstruction steps (please note that the efficiency is always referring to the events collected in the previous selection). Altogether, the reconstruction efficiency to obtain two jets with $p_T > 150$ GeV and a D-meson each, is around 0.06% of the total weighted event. By making use of the ID's of the jets in the PYTHIA event record, we detect whether both jets contain at least one D meson each. Once we select events with two jets containing in these conditions, reconstructed with the PYTHIA event specifications in table 3.1 and the jet specifications in table 3.3.

Restriction	**Efficiency** (selected events weight/total collected events weight)
Events with at least 2 D-mesons	20.7%
Events with at least 2 D-mesons and at least 2 jets	2.073%
Events with at least 2 jets with at least one D each	0.06%

Table 3.4: Efficiency associated to the restriction applied to retrieve the pretended system

The MC truth is obtained with the following procedure: we track the history of the D mesons from both jets until we find the $c/\bar{c}$. If the c-quark is the same for both D-mesons in J1 and J2, we accept the event as MC-truth. In figure 3.4 we present the ΔR distribution of the two jets selected using the method described above. Again we maintain the comparison between the MC-truth and the reconstructed distributions.

The first thing one can immediately notice is the lack of statistics in the distributions in figure 3.4. That is explained by the restrictions explained earlier this chapter to track the D-mesons and the efficiencies obtained in table 3.4. The deltaR distribution itself shows that our results are not consistent with the expectations since we expected the jets containing the D-mesons to be spatially close to one another when in fact they are in opposition to one another. One would expect similar deltaR distributions to the ones in chapter 2.3.3 while the ones we obtained show that the two jets are mostly back to back. One can check this evident peak at π, which means that we are not selecting the pair of mesons we aspired to. By analysing the D-mesons history in the cases that were included in the MC truth scenario, we realised that these were indeed coming from the same c-quark; however, in these cases the c-quark decayed into another gluon which gave rise to another $c\bar{c}$ pair, which in its turn originated another D-meson. Since the algorithm only stops at the last common c-quark, we were not pairing D mesons from the intended system. During this event record assessment, we checked the constitution of each one of the jets used for analysis. The leading jet

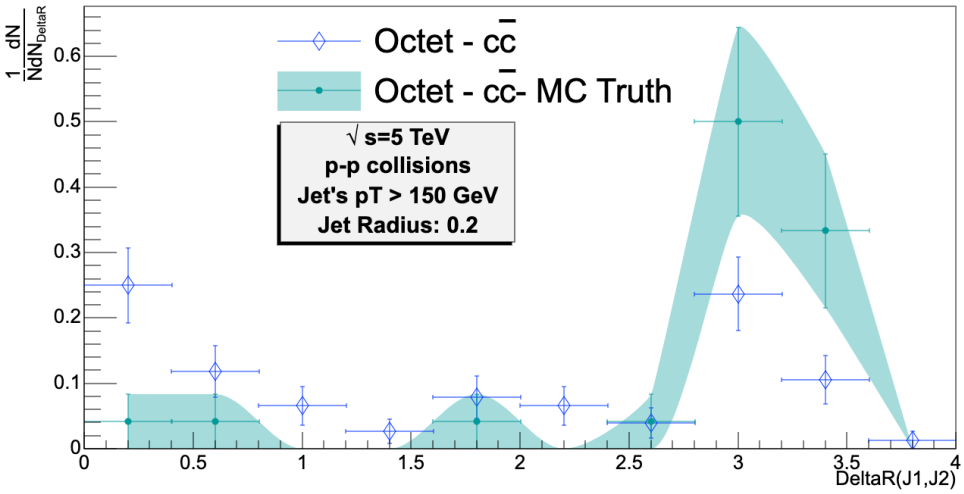

Figure 3.4: Distribution of the deltaR(J1,J2) observable for the D-meson tagging. Uses fully reclustered jets, as our baseline results

always included the D meson pair we were pursuing to find which is consistent with the results in figure 3.3b. That meant we could not pair the mesons through pairing the jets by proximity as we have done until now because they were already paired inside the jet.

For completeness, we also show in figure 3.5 the pull angle distribution for this case for both the reconstructed case and the MC truth. We see a good correspondence between both distributions and also a tendencially flat distribution. We can also see the same tendency as in the octet distribution in figure 2.16. However the amount of events is really small and, from the D-meson deltaR (figure 3.2a) one can see that this method is missing most of the events (which are located at small-R)

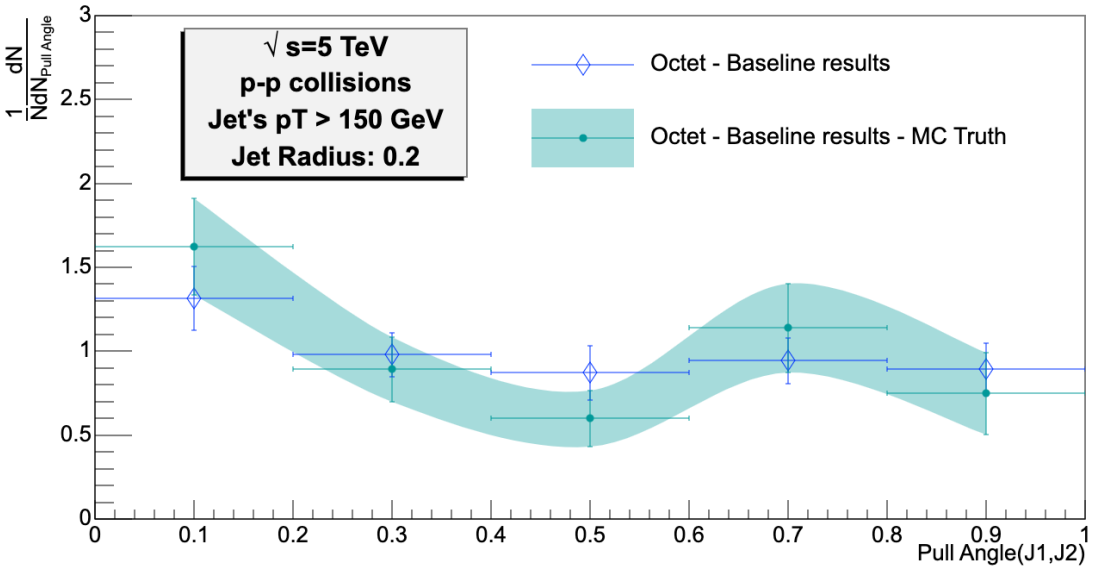

Figure 3.5: Distribution of the pull angle(J1,J2) observable for the D-meson tagging. Uses fully reclustered jets, as our baseline results

In the following section, we will test a different reconstruction method to see if it is possible to tag the

D-mesons on small deltaR which are the ones that will be of more interest for a future HI study.

3.1.2 Subjets method

The method described in the last section did not provide the outcome we expected: we obtained a very small sample of jets containing D-mesons which where positioned back-to-back to one another. To override this, we used the method described in section 2.3.2 and reclustered, using an anti-k_T algorithm and the settings in table 3.5, the constituents of the leading jet into subjets.

	Events
	Octet - $c\bar{c}$
Jet Clustering Algorithm	anti-k_T
Jet Radius	0.4
Reclustering Algorithm	anti-k_T
Subjet Radius	0.2

Table 3.5: The event definition and the input settings of the PYTHIA event for the $c\bar{c}$ case for 2 subjets reclustered from the constituents of the hardest jet in the event

We define jets as settled in table 3.5 and using the event settings in table 3.3 from which we recluster two subjets with radius $R = 2$ using an anti-k_T algorithm from the constituents of the hardest jet in the event containing at least two D meson, that is the jets observed in figure 3.1a. That being said, one can assess the number of subjets inside the hardest jet under the conditions mentioned earlier in figure 3.6a. The subjets, also defined in accordance with table 3.5 are required to have one D-meson each. In figure 3.6b one can check the proportion of subjets containing a D-meson, reconstructed from the jets with ate least one D-meson. Of course that our aim is to target the events which have a jet containing at least two subjets each with one D-meson, from figure 3.6b bars n=2 and n=3.

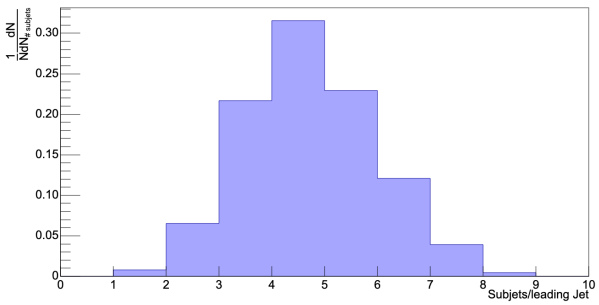

(a) Number of subjets per leading jet containing at least two D-mesons

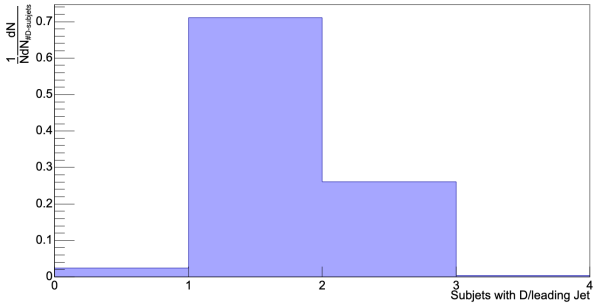

(b) Number of subjets with a D-meson inside the leading jet (with at least two D-mesons

Figure 3.6

We noticed the D-mesons were in the constitution of the leading and subleading subjets of the leading jet of the event (after applying the cuts described before). By checking the particle's ID of the constituents of the leading jet and of its leading and subleading subjets, we confirmed that the majority of events with at least two D-mesons had the mesons in only one jet (more precisely the mesons were part of the leading and the subleading subjet). This is consistent with the results in figure 3.3b where we have arrived to the same

conclusions.The tracking in the event record was possible due to the conjugation of the particles ids and positions in the record with the position and id of the constituents of the subjets, J1 and J2. Then, after making sure that both subjets had one D meson each, we traced the meson's history in the event until we found the common $c/\bar{c}$ from which both mesons should derive; this last step is the difference between the $c\bar{c}$ distributions and the MC truth. The latter uses information on the mesons history, once again, impossible to track in the experiment. In figure 3.7, we show the deltaR distribution of the two subjets under study (leading and subleading subjet of the jet containing two D-mesons) .We see that both the $c\bar{c}$ and the MC truth distributions are in accordance, which proves that with the subjets method we can retrieve the correct system on which we have two D-mesons (one per subjet) each of them coming from the same $c/\bar{c}$ pair.

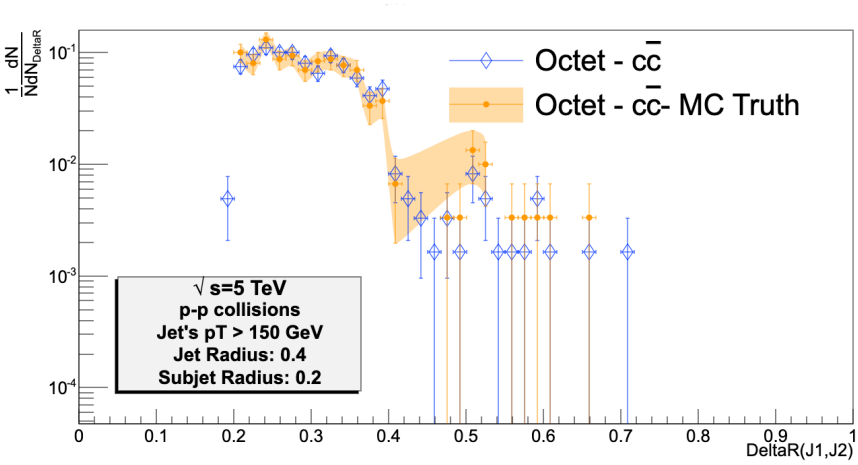

Figure 3.7: Distribution of the deltaR(J1,J2) observable for the D-meson tagging. The MC truth is in accordance with the generic picture of the D tagging

We are now in conditions of applying the pull vector analysis similarly to what we did in the previous section. We kept the comparison between reconstructed results and the MC truth distributions. We start by presenting the pull angle distributions for both the reconstructed and truth level. These distributions are also compared with the baseline results for the octet. We can see them in figure 3.8b

We observe that this tagging helps proving that our standard octet is close to an octet we can control at hadron level. However, we can also see that the behaviour of the D-meson case presents a smoother distribution and it is slightly more peaked at zero than the standard octet (this could include other systems as explained previously). Nevertheless, comparing with the singlet at the pp level, we are still in the presence of a uniform distribution, as expected, and we can also give now evidence of a controlled octet behaviour under the study of the pull vector study.

3.2 Final remarks on the $c\bar{c}$ case

In this chapter we approached a specific octet case, easy to control and to handle at experiment level, in two different ways: by reconstructing two jets and by reconstructing 2 subjets inside the leading jet. We have started from the former approach in order to follow the previous chapter methodology. We have showed

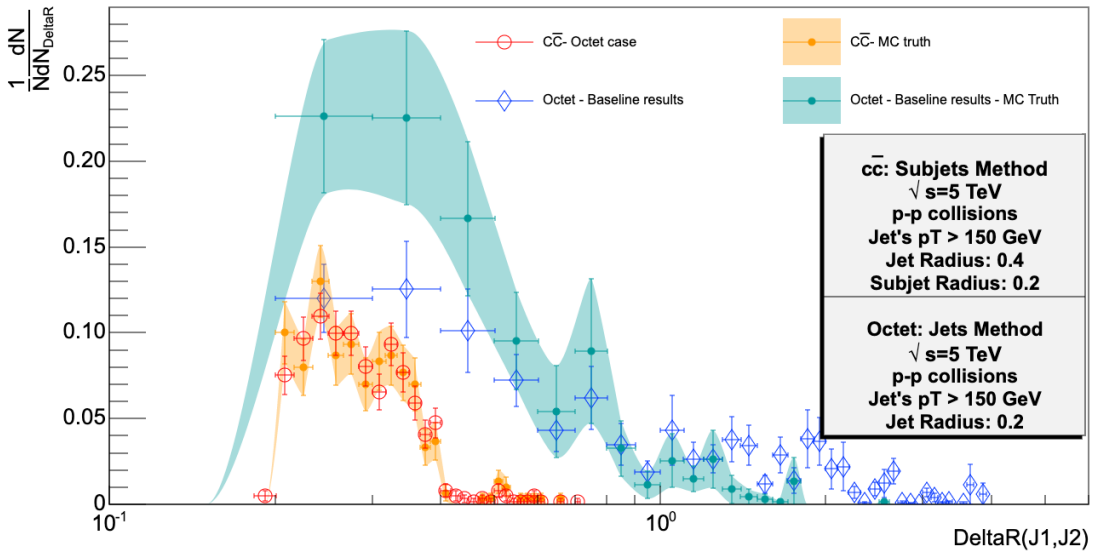

(a) DeltaR(J1,J2) - comparison between our baseline octet results and the $c\bar{c}$ case;

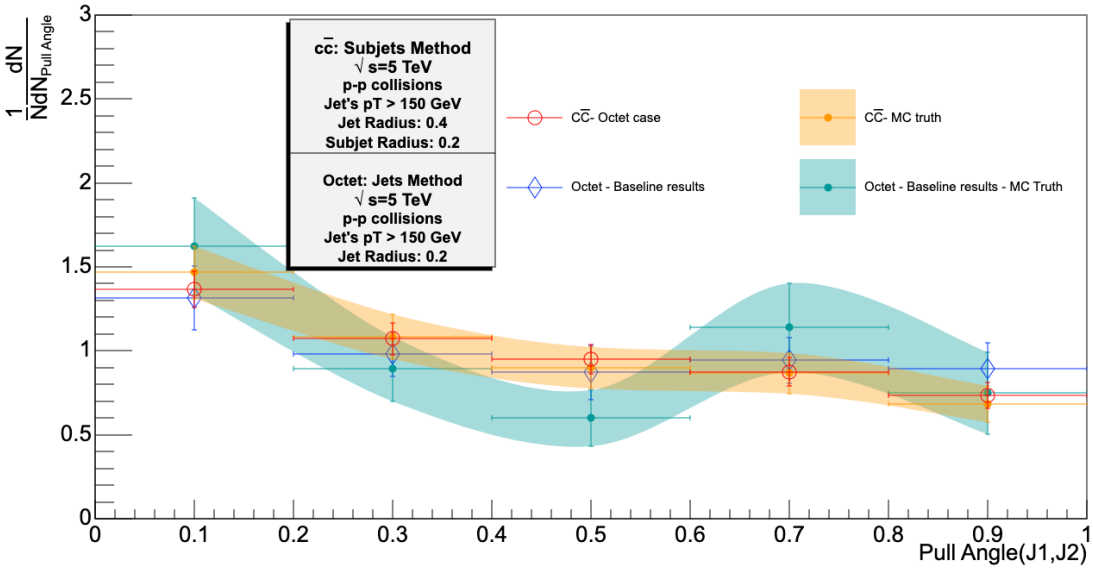

(b) Distribution of the pull angle observable for the D-meson tagging. comparison between our baseline octet results and the $c\bar{c}$ case

Figure 3.8: Comparative picture of our baseline octet and a true octet case (D-meson tagging)

that the requirements we imposed to the events made them hard to get due to the poor efficiency in getting them. Please recall that we require an event with at least two jets and furthermore with one D-meson each. Furthermore, we also conclude that the di-jet system obtained does not fulfil our needs: this analyzes plans to be adapted to heavy ion collisions; in such events we require the D-mesons to be closer to the beam axis in order to avoid the the signal to be spoiled by the background particles (this will be discussed in the following chapter). When one compares the deltaR distribution for the di-jet system with the the deltaR distribution for the two hardest D-mesons per event we can see that we are only getting the residual part of the spectrum close to deltaR $= \pi$ while loosing the dominant contribution close peaking at values close to the jet radius. Adding to this, our studies lead to the conclusion that most of the events with two D-mesons included both of the particles in the same jet's constituents, we adapted the method described previously

on intra-jet reconstruction of subjets. We now see that both issues raised regarding the previous approach are now fixed: we see that proportionality of subjets fulfil our request is more favourable which leads to distributions without major statistical issues, and we now are managing to cover the dominant part of the spectrum of figure 3.2a as one can confirm in figure.

The study developed along this chapter made it possible to build a resilient octet system easy to manage at the experiments and able to be used in an heavy ion environment. Nevertheless the study of the $c\bar{c}$ case also brought strength to our octet system studied in chapter 2. From figure 3.8 we can see the proximity between both sets of distributions. The pull angle distributions are almost coincident with great correspondence between the MC-truth for both cases and between both sets of results. As for the deltaR distributions, we see that they agree on the spatial distribution of the jets/subjets containing the D-mesons to be close to the jets/subjets radius (without forgetting that the distributions are related to different reconstruction methods - confront chapter 2.2.1). This confirms the quality of our octet signal and makes it possible to proceed with the next studies on the pull vector.

Chapter 4

The Pull Vector in Proton-Proton collisions with thermal Background

Now we have the singlet and octet cases that were defined via the decay of colour neutral bosons and the decay of a gluon (chapter 2.2.1), respectively, and also an octet case coming from the gluon splitting into a $c\bar{c}$ pair (chapter 3). We intend now to understand the behaviour of the systems when studied in a situation close to a real heavy ion collision. To do that, we test the resilience of this analysis to the presence of a heavy-ion background. Here the interacting nucleus are represented by Lorentz contracted discs [33]. These are composed by quarks and gluons. When the discs overlap or collide, the incident partons lose energy without falling far apart from the collision centre. The medium-modification of initial multiple parton interactions (MPI) and the underlying event background lead to an higher number of particles produced, when comparing to pp [34] That way the average number multiplicity (number of particles produced in the event) is considerably higher in HI with respect to pp [35]. We are going to use with a toy MC to simulate the background particles of an HI event where the pp event simulated via PYTHIA (tab. 4.1) will be embedded. We start by describing the background generation process (section 4.1) and explore the influence this background plays in the systems explored in the previously in section 4.2. We will also study two different particle subtraction methods and further develop the most appropriate one for our purpose.

	Events	
	Singlet	Octet
Channel	Double boson hadronic decay (Z and W bosons)	Gluon splitting
PYTHIA Channels	**WeakDoubleBoson**:all	**HardQCD**:gg2gg and **HardQCD**:qqbar2gg
Particle's minimum pT	0.5 GeV	
Particle's eta range	[-3,3]	
Minimum Jet p_T	150 GeV	
Jet's η range	[-2.5,2.5]	
Mass (J1+J2)	[70,120]	-
Jet Radius	0.2	

Table 4.1: Thermal background Pythia events settings

4.1 Thermal Background: Settings of the background

In [36], the ALICE experiment determined the number of charged particles for Pb-Pb collisions at $\sqrt{s_{nn}} =$ 5.02TeV. There, they show that in the most central region, [-3.5, 5] in pseudorapidity, one has about 18000 charged particles (figure 4.1).

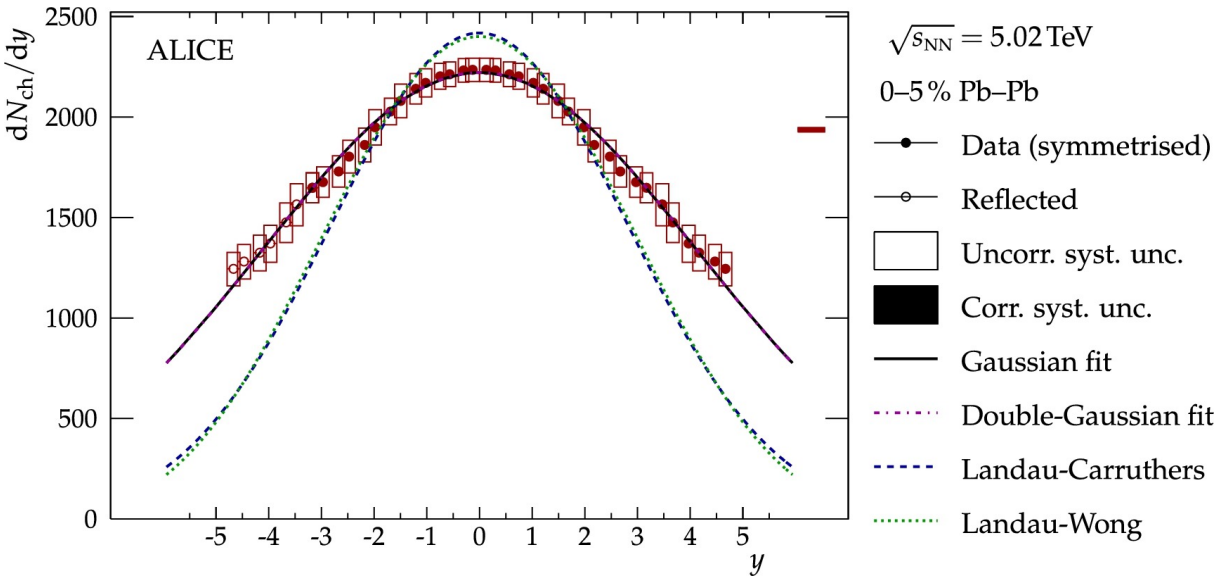

Figure 4.1: Density of background particles in the most central (0–5%) Pb–Pb collisions at $\sqrt{s_{nn}} =$ 5.02TeV [36]

This is a very qualitative approximation, because the particle distribution is not homogeneous in that large gap of pseudorapidity. In order to use this information in our background studies on the observable pull vector, we use a toy MC which simulates particles according to a thermal spectra. In figure 4.2a we plot the p_T spectrum of the background particles as well as the p_T spectrum of the PYTHIA event particles with the settings in 4.1 (figure 4.2b).

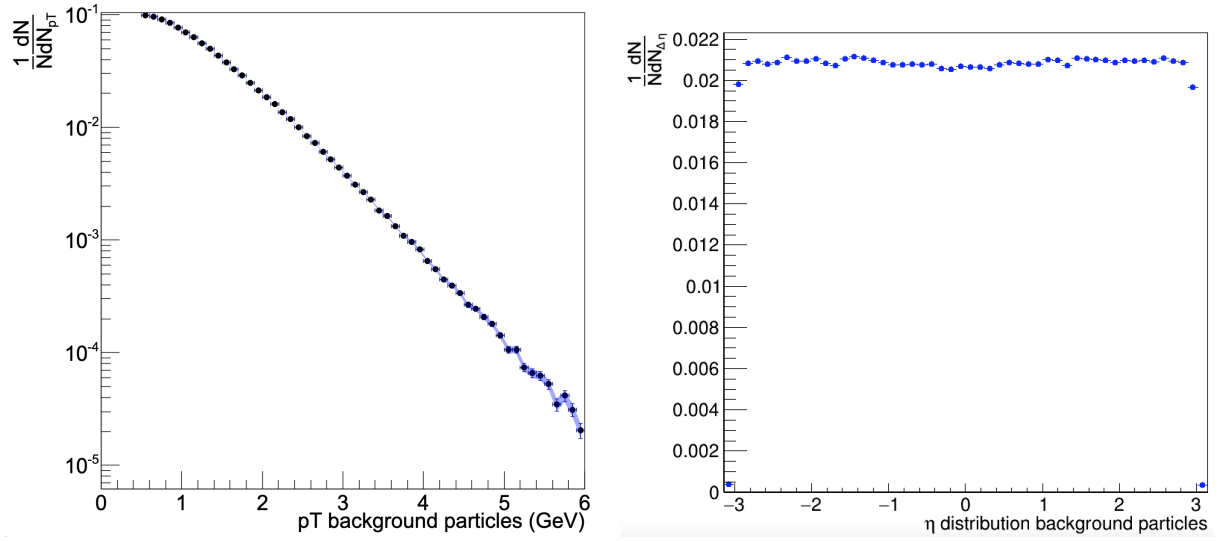

(a) pT spectrum for the thermal background particles

(b) η distribution for the background particles

Figure 4.2: Background particle's profile

The size of the background population per event follows a gaussian distribution with average 18000. This figure is obtained by approximation, based on the information provided in [36]. That way approximately 2000 charged particles per unit rapidity is a good estimate. We are working in a pseudorapidity range [-3,3] and one must consider a 3/2 factor to include neutral particles, one obtains the average number N=18000 (which is obtained by considering the 2000 particles/η for the 6 units in η contained inside our frame and the 3/2 term to account neutral particles, and not only charged ones). The background particles are generated with p_T given by the probability distribution function given in table 4.2, where we collect all the settings used to generate the background particles. There we establish the minimum p_T of background particles as 0.5 GeV, so as to stay in accordance with the minimum p_T required for the particles in the PYTHIA event (table 4.2). In figure 4.2 we present the thermal p_T spectrum of the background particles (left), together with the η distribution between [-3,3], which we can confirm is uniform in the range of the referred interval.

With such settings we obtain a thermal background similar to the one seen in ALICE and that mimics the effect of a Pb-Pb collision at $\sqrt{s} = 5$ TeV (figure 4.1). This is what is usually called a simplified model of a heavy-ion background since dedicated heavy-ion Monte Carlo event generators are available. But, for the purpose of this exercise, it suffices to see how uncorrelated particles affect the pull angle signatures for the referred systems to predict whether the coherence effects we observe in pp will still maintain in HI collisions.

pT	**η range**	**Φ range**	**min. pT**	$\bar{N}$
$xe^{-x/0.5}$, $x \in [0, 400]$	[-3,3]	[-π,π]	0.5 GeV	18000

Table 4.2: Thermal background particles settings

The thermal background is embedded to the PYTHIA event particles ensemble. In figure 4.3 we have represented the jets' transverse momentum spectrum prior and after the introduction of background.

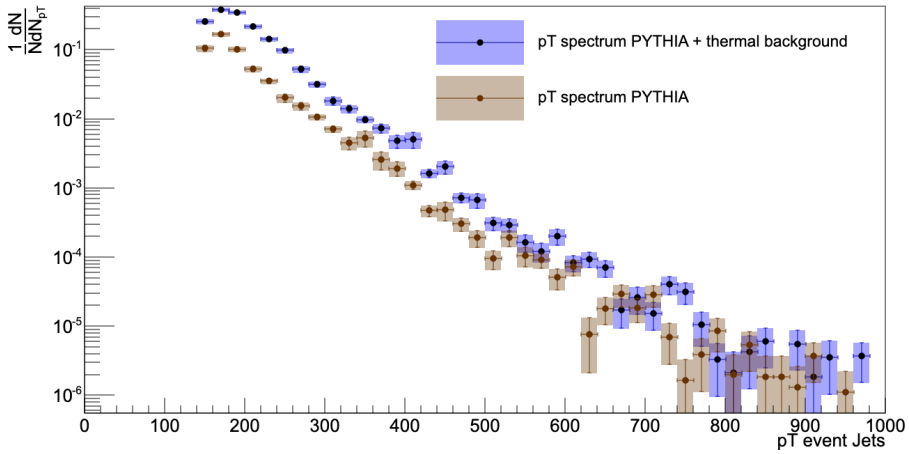

Figure 4.3: Jet's pt distribution with and without the influence of the background

We can see that there is a clear shift in the distribution. This matter will be addressed further in chapter 4.3 where we will discuss further techniques to assess whether the background is properly set up. One can then test the effect of embedding background particles in the behaviour of our observable.

4.2 Effects of background in the observable

Now that one established a background capable of mimic a Pb-Pb collision background, one can proceed to compare the effect that such background plays in the behaviour of the pull angle observable. One should first inquire what one expects from the addition of the background particles. The effect in the singlet is expected to be significant: one predicts that the strength of the signal showing a colour connection between the quark-anti-quark system should decrease. As we mentioned earlier, the addition of thermal particles to the event will not affect the magnitude of the vector but only its direction, that is the pull angle. The newly added particles are expected to weaken the colour bond between the singlet jets since we add uncorrelated particles with no colour connection with the existing ones and among each other. As for the octet the same is not expected. The octet is identified by the lack of existing colour bonds amongst jets: we are adding particles with no colour bonds to the event so they will not play any difference in the pull vector direction. Nonetheless these effects will now be investigated in the remainer of the present chapter.

4.2.1 Singlet

Let us start by embedding the background particles in the events obtained for the singlet case as described in 2. Our purpose now is to compare the results in the previous chapter with the new results under the influence of a thermal background. For doing so, we present the results on deltaR (fig. 4.4a) and pull angle distribution (fig. 4.4b) for the singlet event with thermal background case with (the orange shaded plot) and without (the red scatter plot) the mass cut we introduced when reconstructing the singlet. We then compare, in the same figures, these results with our pure singlet event (the blue shaded plot) obtained in chapter 2. Recall that the event is generated with the cuts in table 4.1. The p_T cut applied to the jets is performed after adding the background particles to the PYTHIA event. The clustering procedure with the anti-k_T method and the requirements in 4.1 follows these background embedding and includes both the event's and the newly added thermal particles.

We can see that by applying the mass cut the deltaR distributions became similar to each other, which comes from using the same reconstruction method and an anti-k_T algorithm which, as we mentioned earlier, tends to merge hard particles. We also see that the mass cut is responsible for bringing the system closer to the system with no background influence. In terms of the pull angle distribution, we can observe that in figure 4.4b, the pull angle suffered a major decrease in showing the connection between the two prongs - there is not a pronounced peak at pull angle zero for the signal of the event + embedded background case. Based on these results, one argues that the addition of the background will be sensed mostly in the colour flow direction, that is, in the pull angle, since the pull angle did not react the same way as the deltaR distribution.

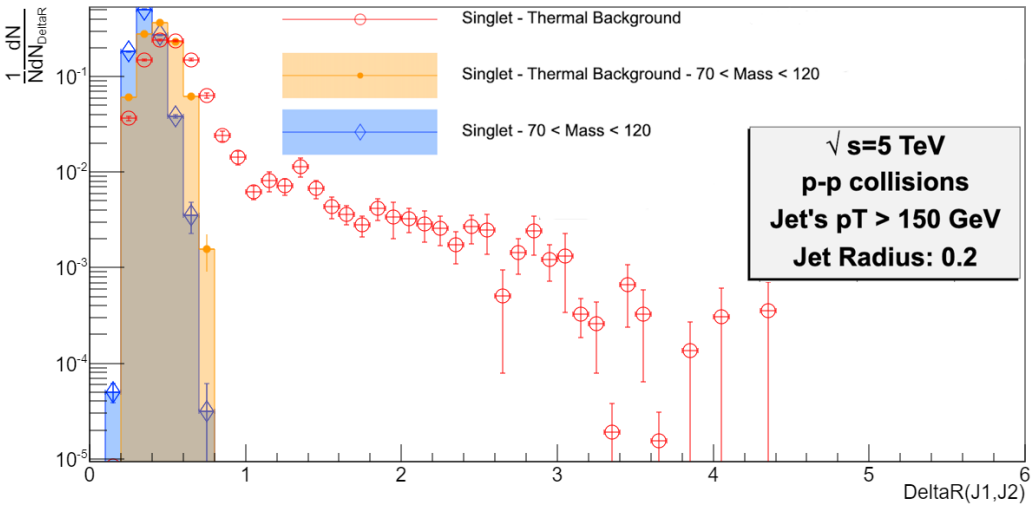

(a) DeltaR(J1,J2) - comparison between our baseline results and the singlet case with thermal background; we see that by imposing the Mass window cut we retrieve a similar distribution to the baseline

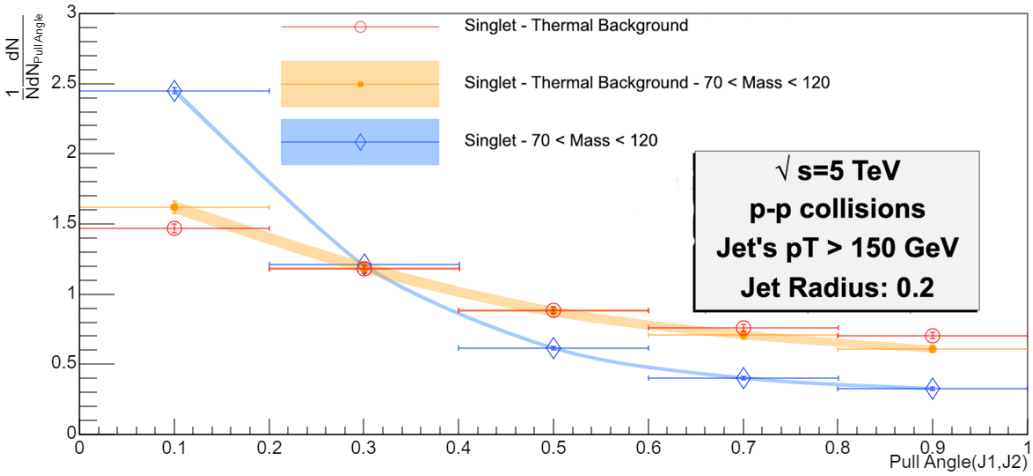

(b) The pull angle for the singlet case with thermal background gets way apart from the baseline distribution; even introducing the mass window cut would not bring the distributions close to each other

Figure 4.4: Comparative picture to assess the effect of background introduction in the singlet system and also the effect it plays in the observable

4.2.2 Octet

In this section we assess what is the effect that the embedded thermal background plays in the octet baseline system - the the $q\bar{q}$ resulting from gluon splitting which we established in chapter 2.2.1. In figure 4.5, we compare the results from chapter 2.2.1 (blue shade) with the embedded background in the same system (orange shade) for the deltaR and the pull angle distributions. In this case no mass cut is applied but we reconstruct all anti-k_T jets with $R = 0.2$ above a $p_T \geq 150$ GeV in $|\eta| < 2.5$.

We observe that the octet, as it is defined, is not affected by the introduction of background. That is, by adding thermal background particles in the event our octet signature in the pull angle behaviour does not change.

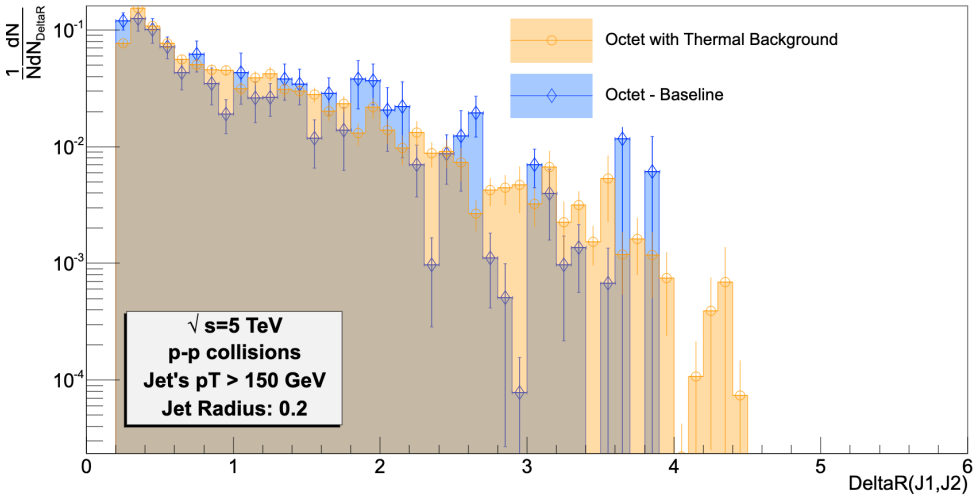

(a) DeltaR(J1,J2) - comparison between our baseline octet results and the octet case with thermal background;

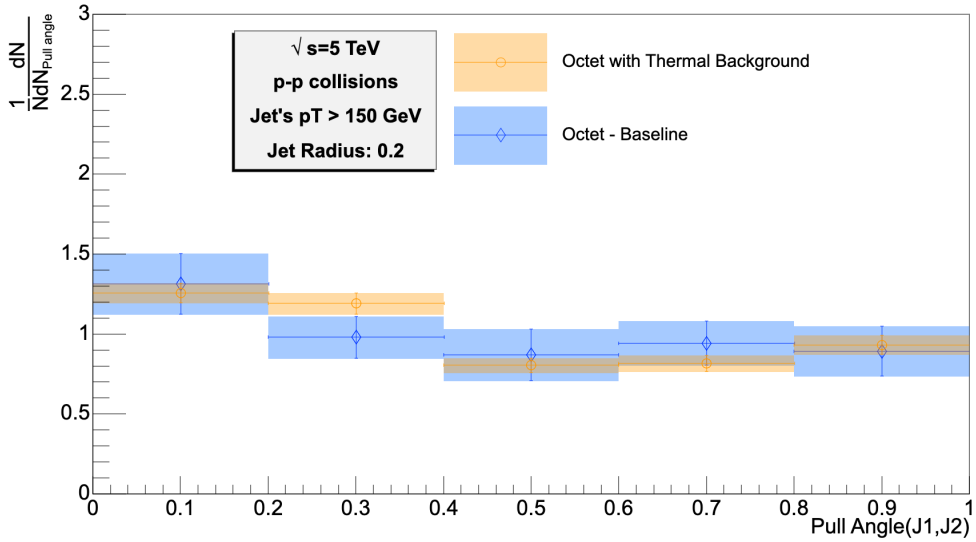

(b) Pull angle distribution

Figure 4.5: Comparative picture to assess the effect of background introduction in the octet system and also the effect it plays in the observable

4.2.3 The Octet $c\bar{c}$ case

We introduced in chapter 3.1.2 an octet case closer to the one of interest for HI studies dedicated to colour (de)coherence: the $c\bar{c}$ case. We shall revisit now this case where we look into jets with two subjets each with one D-meson, and determine the pull vector. As we have seen in chapter 3, the optimal event reconstruction method differs from the ones approached in the course of this chapter due to the fact that one would find the D-meson pair in a single jet. In this section we will focus on the effect that the thermal background into a PYTHIA event when looking to the pull angle from a $g \rightarrow c\bar{c}$ radiation, in the behaviour of the observable.In figure 4.6a we analyze the deltaR distribution for the $c\bar{c}$ case with (in orange) and without (in blue) thermal background and in figure 4.6b the same comparison but now for the pull angle distribution.

The distributions show us that the deltaR distributions are quite close to each other which is consistent with the results we obtained in the last two sections (despite showing difference in the behaviour of the pull

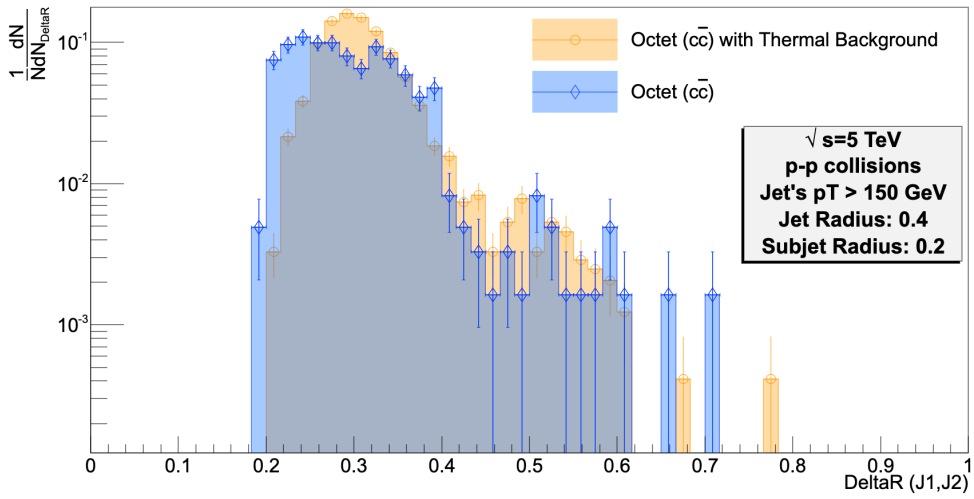

(a) DeltaR(J1,J2) - comparison between $c\bar{c}$ octet case results with and without thermal background;

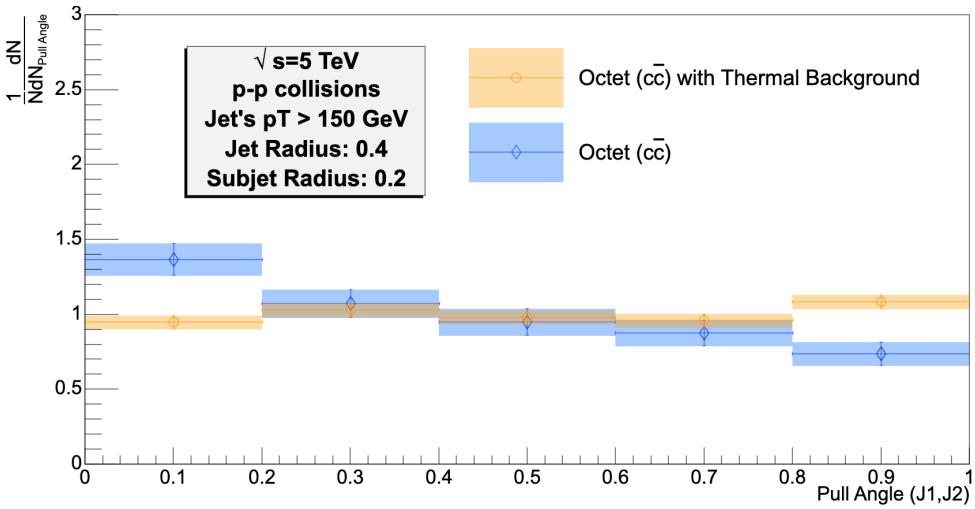

(b) Pull angle distribution

Figure 4.6: Comparative picture to assess the effect of background introduction in the octet $c\bar{c}$ system and also the effect it plays in the observable

angle observable also observed for the baseline singlet case, the spatial description of the system remains similar before and after of the addition of background particles). We notice that the introduction of the background flattens the pull angle distribution in the case of the $c\bar{c}$ case. This means that this system is more sensitive to the presence of background than the baseline octet we studied in the last section, were we did not observe such variations in the pull angle distribution due to the embedding of background particles in the event.

4.3 Background Subtraction - methods

Following the considerations of last section regarding the fading of pull angle signal for the singlet one must turn to a solution to retrieve our observable in conditions able to be applied in the experiment.

At the LHC protons, collide with an enormous instantaneous luminosity. This is a requirement to find

novel physics processes. However such conditions generate a contribution from multiple pp interactions, uncorrelated with the signal - pileup. However at calorimeters there is not such angular sensitivity. This enforced the application of corrective measures to the pileup phenomena. In [37] *jet-by-jet* and *event-by-event* background subtraction methods are introduced. These are area based methods which enforce a 4-momentum correction to the jets, to account for the pollution provided by soft constituents contribution.

4.3.1 Area based methods

One can perform an additional check to confirm whether the results are consistent. The δp_T observable is determined using:

$$\delta p_T = p_{T\,Pythia+background} - p_{T\,Pythia} - \rho \times Area, \tag{4.1}$$

where ρ stands for the background density per unit area. This observable is a way to understand the overall contamination within the jet area. It also allows to correct the jet scalar p_T spectrum, to account the presence of the density of background particles. In this case we used a simple area based background subtraction, given in [37][25]. As one may conclude, there is the need to guarantee the correspondence between PYTHIA jets and PYTHIA+background jets. In order to achieve the correspondence we perform as follows:

1. a first clustering of the PYTHIA particles solely with an anti-k_T algorithm, $R = 0.2$ and $p_T \geq 150$GeV;
2. a second clustering of the PYTHIA+background case using the same clustering settings;
3. check the deltaR between jets in item 1 and jets in item 2;
4. determine the distance between the jets with background particles relatively to each of the jets without background, and we pair the closest PYTHIA jet to the PYTHIA+background jet;
5. compute the formula in eq. 4.1.

In figure 4.7 we subtract the p_T of the PYTHIA event particles and the prediction of background to the p_T of the PYTHIA+background system. Additionally, we also fit a gaussean function to the distribution in order to retrieve the gaussean parameters (the fit results are in table 4.3). The jets considered concern the entire PYTHIA event for the event and jet reconstruction restrictions we show in table 4.1 in a p_T window [150,170] GeV and the sum of the PYTHIA event to the thermal background described above (PYTHIA + background) to which we perform the same clustering procedure with the same restrictions. That way we can assess the influence of the background in the p_T spectrum of the overall event and complement the information in 4.3 (we already checked the spectrum would suffer a shift but we will now quantify the shift).

σ	$\bar{X}$
9.3 ± 0.1	0.7 ± 0.2

Table 4.3: Fit parameters of the δp_T distribution to a gaussean function

Due to the fact that we are considering jets with radius $R = 0.2$, the effect of the background particles is rather small, leading to a narrow δp_T of a few GeV. However the prediction in [36] would be of a $\sigma \approx 5$ GeV. As we can see in our case the same quantity is about 9 GeV which shows us we are slightly off the expected value, which means our sample is more contaminated by the background. The mean value of the gaussean stands $\mu_m ean \approx 0$ which means that the subtractor is well defined. However our major issue with this method is indeed this area based background subtractor. The problem with these area-based methods is that they are not possible to apply in our specific case due to the particle by particle nature of our observable. That way one require a method that would act at particle-level to remove the background event from our jets co recover the colour coherence relations. Such methods exist and are called constituents subtraction methods and will be studied in the next chapter.

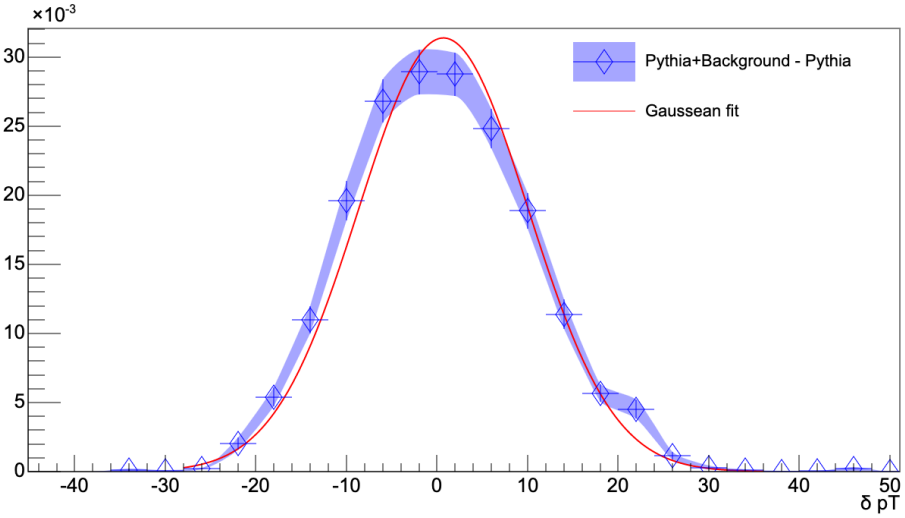

Figure 4.7: We perform a fit to the δpT distribution with background estimation obtaining:$\sigma = 9.3 \pm 0.1$, $\bar{X} = 0.7 \pm 0.2$

4.3.2 Constituent Subtraction

In chapter 4.3.1 we used an area based method to remove background on average. We also obtained the δp_T distribution. As we concluded these area based methods are not suitable to our study of colour coherence between jets. Thankfully, novel approaches to the pileup issue have been addressed in [38]. Here are provided the steps to achieve a modified method which apply modifications directly in the jets constituents. It is also relevant because it is independent of the jet reconstruction algorithm. That way, it is useful in heavy ion collisions on which jet reconstruction is a more demanding process. As the name might suggest, the 4-momentum corrections are applied to each particle, changing at the same time both jet's structure and substructure. This is achieved by adding ghost (massless) particles to the event, usually used to assess the area of jets. Then a clustering is performed and on obtains jets but now also with ghost particles in its constituents. We can now use the ghosts to correct the pileup effects in each jet: the algorithm sets the ghosts pt to negative values, and matches ghosts to event particles on a deltaR basis. Next the mass and

4-momentum correction is applied. That way we have a robust method to retrieve our pull angle singlet signals. The method is already implemented in the contribution package of FastJet and we will make use of it.

Let us revisit the δp_T distribution now using the particle level subtraction method: we compute the observable by supplying the result of the background subtraction and the PYTHIA event particles as input. The result is plotted in figure 4.8, where we once again plot the δp_T distribution and make a gaussean fit (table 4.4) to the distribution to retrieve the σ value.

σ	$\bar{X}$
6.9 ± 0.1	1.9 ± 0.2

Table 4.4: Fit parameters of the δpT distribution to a gaussean function

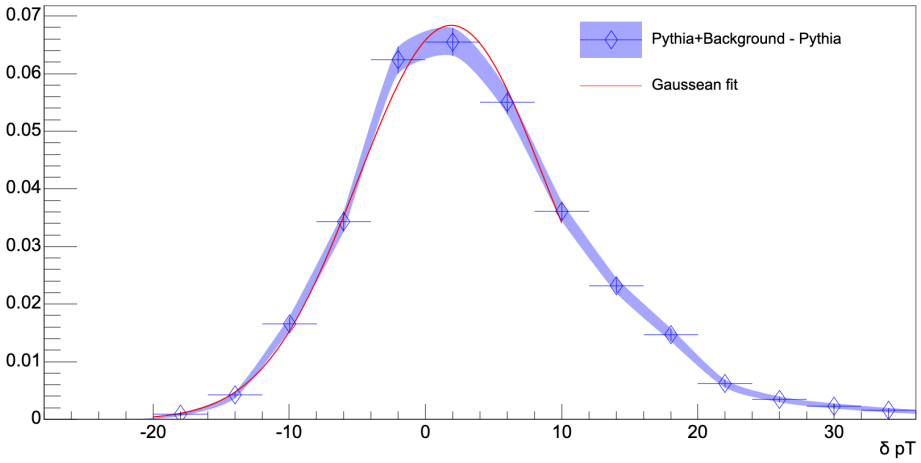

Figure 4.8: We perform a fit to the δpT distribution with background subtraction obtaining:$\sigma = 6.9 \pm 0.1$, $\bar{X} = 1.9 \pm 0.2$

Once again we have a gaussean distribution with center close to zero, which shows that our background subtraction is working, similarly to what was previously discussed in the last section. On the other hand we now have a closer σ to the predicted value for Pb-Pb collisions at $\sqrt{s} = 5$TeV which is around $\sigma = 6.5$, which means that our jets only fluctuate ± 6.5 GeV with respect to their truth p_T value.

4.4 Pull Angle with Thermal Background Subtraction

As we have seen in the previous chapter the *particle-by-particle* subtraction is the most appropriate to apply due to our observable characteristics. That way, to retrieve the behaviour we saw in vacuum, we use a particle level subtraction algorithm. It is then time to return to our observable and specifically to our pull angle results and apply this constituents subtraction method to bypass the effects of the thermal background.

4.4.1 Singlet

Returning to the singlet case, in figure 4.9, we analyze this approach by checking once more the deltaR distribution and the pull angle distributions.

Recall from the previous section that our main problem was that the singlet signal was masked by the introduction of thermal background even though deltaR was similar to the singlet distribution without background. We observe that we now manage to get a similar picture with thermal background subtraction to our baseline results, that is, we managed to get our signal out of a medium filled with soft background. On top of that, by implementing the mass window cut [70, 120] GeV we applied to our baseline results, we obtain even close results, which impels to conclude that the singlet signal survives in the presence of a HI background.

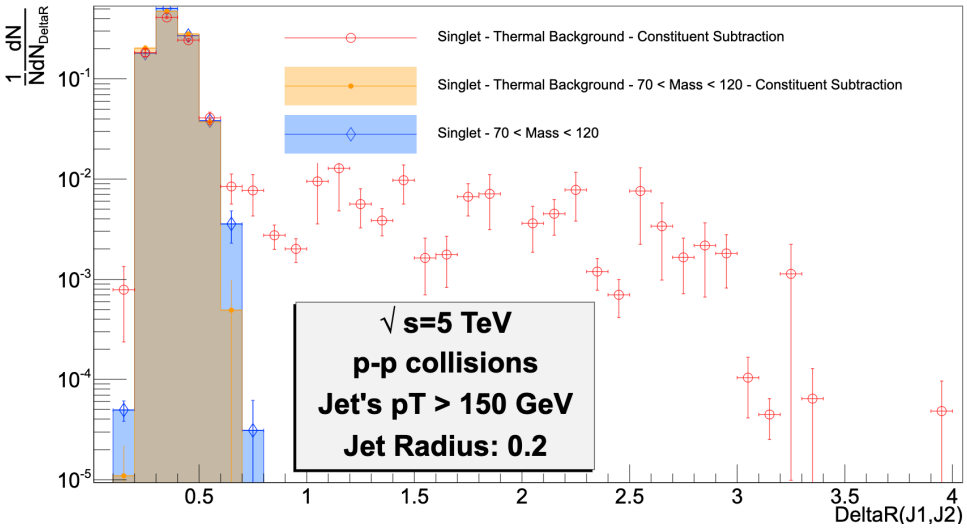

(a) DeltaR(J1,J2) - comparison between our baseline results and the singlet case with thermal background after constituent subtraction; we see that by imposing the Mass window cut we retrieve a close distribution to the baseline one

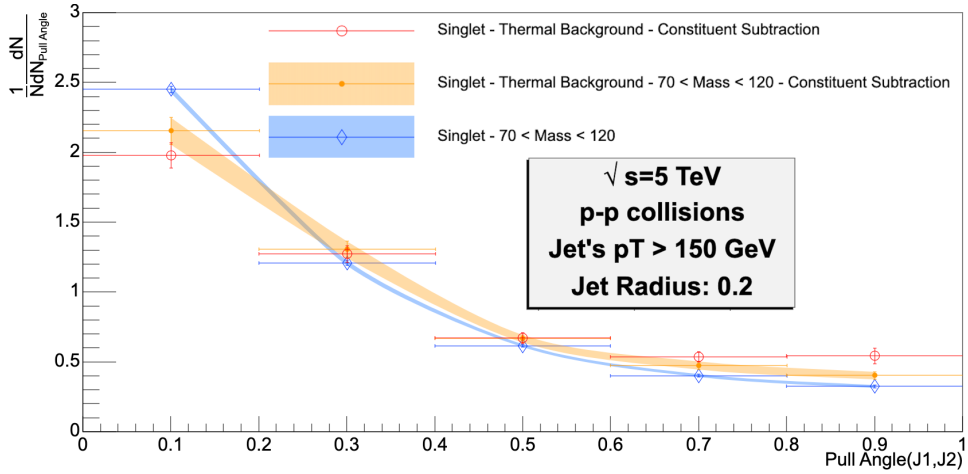

(b) The pull angle for the singlet case with thermal background after constituents subtraction gets really close to the baseline distribution; introducing the mass window cut improves the results

Figure 4.9: Comparative picture to assess the effect of background introduction after background constituent subtraction in the system and also the effect it plays in the observable

4.4.2 Octet

We also study the constituents subtraction in the octet system. This served as a benchmark on how close the pull angle distributions referring to both systems - octet and singlet - would get to one another. In other words it helped us assessing whether we were getting in a situation where singlet and octet could no longer be distinguished by analysing the pull angle distribution. That way, in figure 4.10, we compare the octet under the thermal background influence and after constituents subtraction with the baseline octet (chapter 2.2.1). We do these comparisons for the deltaR distribution (figure 4.10a) and the pull angle distribution (figure 4.10b).

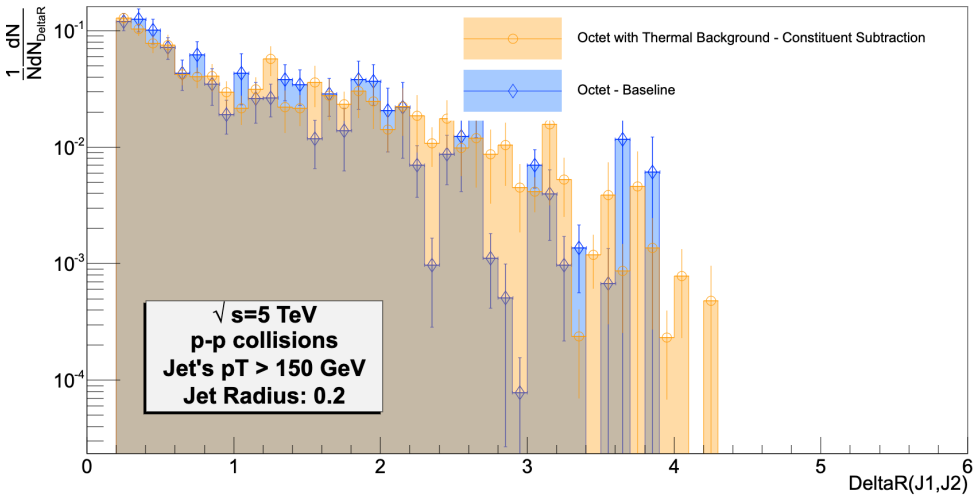

(a) DeltaR(J1,J2) - comparison between our baseline results and the case case with thermal background after constituent subtraction;

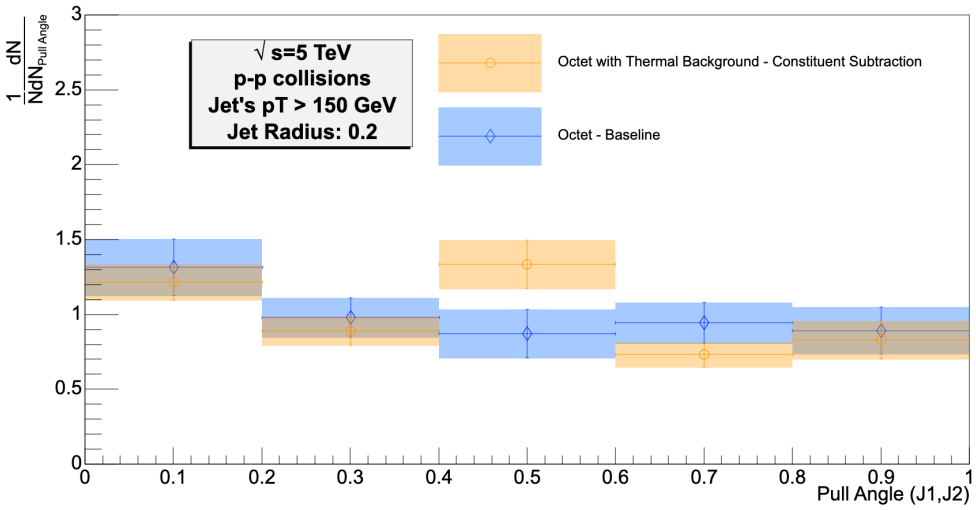

(b) The pull angle for the case case with thermal background after constituents subtraction

Figure 4.10: Comparative picture to assess the effect of background introduction after background constituent subtraction in the system and also the effect it plays in the observable

From the results we obtained above it is clear that performing the constituent subtraction step is not that relevant in the case of the octet. Nevertheless it will also not induce any biases and the flat distribution survives.

4.4.3 The Octet $c\bar{c}$ case

In chapter 4.2.3, we analyzed the effect that the background particles played in the behaviour of the pull vector when applied to this system. Since we noticed a significant difference in the pull angle observable we now intend to apply the background subtraction method used in the previous sections to retrieve the original signal observed without background. For that we compare the results after subtracting the background with the baseline results in figure 4.11: in figure 4.11a we present the deltaR distribution for both cases, and in figure 4.11b the pull angle distribution.

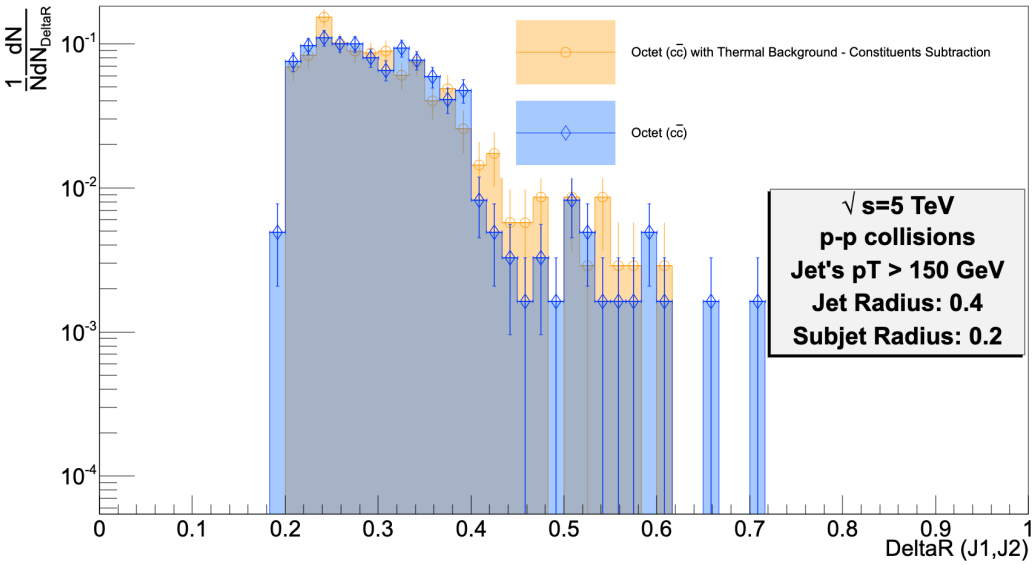

(a) DeltaR(J1,J2) - comparison between $c\bar{c}$ octet case results with and without thermal background;

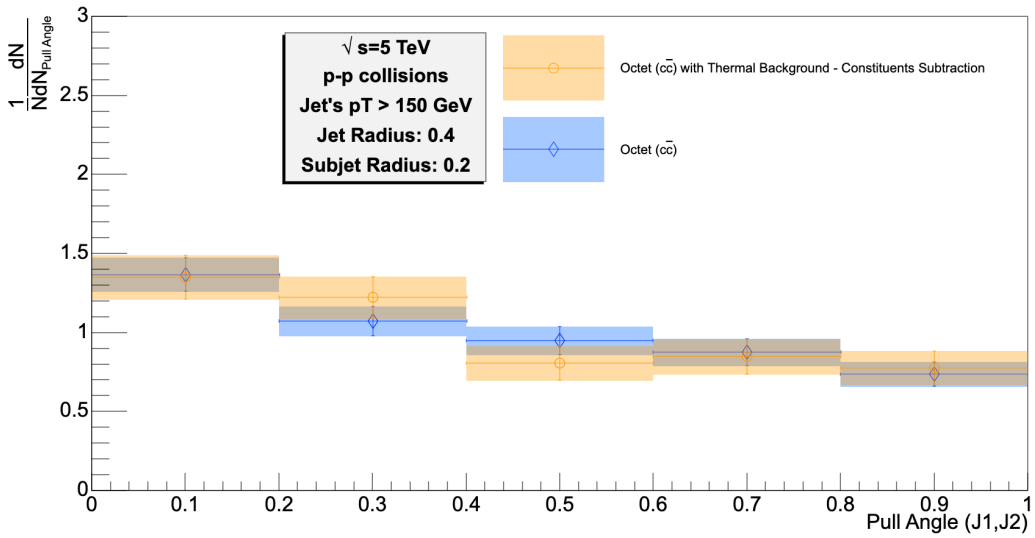

(b) Pull angle distribution

Figure 4.11: Comparative picture to assess the effect of background after constituent subtraction in the octet $c\bar{c}$ system and also the effect it plays in the observable

It is clear to see that the deltaR distribution after subtraction is almost identical to the distribution without any use of background. For the pull angle case, we observed in chapter 4.2.3 that the thermal background influenced the pull angle distribution. The constituents subtraction method solves this discrepancy and we manage to retrieve the original signal.

Chapter 5

Conclusions and final remarks

The aim of this thesis was to study the feasibility of colour coherence studies using the jet pull in heavy ion collisions. The study consisted on three main points

1. The development of an algorithm to select colour octet and singlet configurations in pp collisions. Those algorithms were applied to simulations at detector level and validated with the MC truth. Different approaches based on small-R jet reconstruction and jet substructure were considered. Two alternative octet configurations were chosen: a gluon splitting into a $c\bar{c}$ and and a simple gluon to gluon emission in di-jet events.

2. The analysis of the jet pull angle observable and its distinct features in singlet and octet systems.

3. A study of the impact of the large heavy ion background on the jet pull angle differences between singlet and octet configurations.

For that, throughout this thesis we present a study of intra-jet colour coherence effects in pp collisions at $\sqrt{s} = 5$ TeV. We use the jet pull vector, more specifically the jet pull angle, to perform this study. The pull angle conserves information regarding the direction of the colour flow, and presents a distinct signature as it peaks at zero in the presence of a colour singlet (interconnected jets) and presents a uniform distribution in the presence of a colour octet. This observable was previously explored as a means to identify the colour structure of the initiated jet. In this thesis, we use it as a novel tool for heavy-ion studies, namely to identify if indeed colour decoherence is manifested in heavy-ion collisions. This required several steps as follow.

The colour decoherence studies require a physically closed system, with a small distance between the prongs in study. This opposes to the systems used in existing studies. For that reason, in chapter 2 we achieve to establish baseline systems of a colour singlet (double boson weak decay) and a colour octet (hard QCD events with a gluon pair coming form the hard scattering) fulfilling our proximity needs. This results are to be the benchmark for all the remaining results we present. One then requires them to be well distinct from one another to fulfil that role. As we presented in the same chapter, we managed to identify the singlet and octet cases by going to high-p_T jets, and using either small-R jets or subjets. We also concluded

that the prior were likely to perform better in the presence of a background, due to the greater difference experienced between the octet and singlet signals.

The prospects of this work have a larger reach than pp collisions in vacuum: the goal is to extend it to heavy ion collisions. From a highly populated environment, the octet system will be hard to be identified out of the bulk (since jets uncorrelated to the hard scattering can be produced). As such, identifying heavy particles - that are more difficult to be produced outside hard scattering fragmentation - can be a solution to have a clear octet system (with the necessary conditions to test colour coherence) in a heavy-ion environment. D-mesons are a very useful probe since they come from a c-quark, which is the lightest of heavy quarks. As such, it can be produced via gluon splitting into a $c\bar{c}$ pair. In this case, the D-mesons that would come from the same gluon splitting were often found very close to each other (within the same small radius jet). Without a suitable two-object system it was not possible to identify the pull vector. As such, in this chapter, we demonstrate that an octet system possible to be experimentally identified in a heavy-ion environment need to be defined via jet substructure. In particular, the best method was to reconstruct subjets from within the fully reconstructed jets. We obtained an octet signal slightly less uniform than the baseline but still with a great proximity to the truth MC distributions and well distinct to the singlet, with a sharp peak at zero.

Finally we showed the effects that a thermal background, tuned to mimic a realistic Pb-Pb collision at $\sqrt{s} = 5.02$ TeV, plays in the pull angle observable for the 3 systems: singlet, octet (hard QCD events) and $c\bar{c}$. As expected, with the introduction of soft particles, the singlet and the two octets become almost indistinguishable. Because of this, we introduced a constituents background subtraction method aimed to increase our pull angle signature and applied to the three systems. The results showed that we can retrieve the baseline signals of pull angle and, in extension, of colour coherence, with a subtraction method available at current experiments (instead of: experimental level.)

To sum up we developed the tools and methods that will allow to check if colour coherence effects can be identified in an event with a thermal background influence as the one present at Pb-Pb collisions at $\sqrt{s} = 5$ TeV. This is achieved by using subjet reclustering methods out of fully reconstructed jets and subtraction methods, with which one can retrieve the vacuum proton-proton signatures characteristic of a colour octet and a colour singlet. Our studies conclude that the differences survive the heavy ion background after subtraction techniques are applied.

Bibliography

[1] A. B. Arbuzov, "Quantum Field Theory and the Electroweak Standard Model", pp. 1–34, 2017. arXiv: 1801.05670 [hep-ph].

[2] M. Gell-Mann, "A Schematic Model of Baryons and Mesons", *Phys. Lett.*, vol. 8, pp. 214–215, 1964.

[3] L. Apolinário, Y.-J. Lee, and M. Winn, "Heavy quarks and jets as probes of the QGP", Mar. 2022. arXiv: 2203.16352 [hep-ph].

[4] Y. Dokshitzer, *Basics of Perturbative QCD*, ser. Basics of. Editions Frontières, 1991.

[5] J. Casalderrey-Solana, Y. Mehtar-Tani, C. A. Salgado, and K. Tywoniuk, "New picture of jet quenching dictated by color coherence", *Phys. Lett. B*, vol. 725, pp. 357–360, 2013. arXiv: 1210.7765 [hep-ph].

[6] Y. L. Dokshitzer, V. A. Khoze, and S. I. Troian, "On specific QCD properties of heavy quark fragmentation ('dead cone')", *J. Phys. G*, vol. 17, pp. 1602–1604, 1991.

[7] S. Acharya *et al.*, "Direct observation of the dead-cone effect in quantum chromodynamics", *Nature*, vol. 605, no. 7910, pp. 440–446, 2022. arXiv: 2106.05713 [nucl-ex].

[8] G. P. Salam, "Towards jetography", *The European Physical Journal C*, vol. 67, no. 3-4, pp. 637–686, May 2010.

[9] M. Cacciari, G. P. Salam, and G. Soyez, "The anti-k_t jet clustering algorithm", *JHEP*, vol. 04, p. 063, 2008. arXiv: 0802.1189 [hep-ph].

[10] L. Apolinário, A. Cordeiro, and K. Zapp, "Time reclustering for jet quenching studies", *Eur. Phys. J. C*, vol. 81, no. 6, p. 561, 2021. arXiv: 2012.02199 [hep-ph].

[11] M. Cacciari, *Phenomenological and theoretical developments in jet physics at the lhc*, 2015. arXiv: 1509.02272 [hep-ph].

[12] B. Andersson, G. Gustafson, G. Ingelman, and T. Sjostrand, "Parton Fragmentation and String Dynamics", *Phys. Rept.*, vol. 97, pp. 31–145, 1983.

[13] T. Sjostrand, S. Mrenna, and P. Z. Skands, "PYTHIA 6.4 Physics and Manual", *JHEP*, vol. 05, p. 026, 2006. arXiv: hep-ph/0603175.

[14] T. Gleisberg *et al.*, "Event generation with SHERPA 1.1", *JHEP*, vol. 02, p. 007, 2009. arXiv: 0811.4622 [hep-ph].

[15] M. Bahr *et al.*, "Herwig++ Physics and Manual", *Eur. Phys. J. C*, vol. 58, pp. 639–707, 2008. arXiv: 0803.0883 [hep-ph].

[16] J. Bellm *et al.*, "Herwig 7.0/Herwig++ 3.0 release note", *Eur. Phys. J. C*, vol. 76, no. 4, p. 196, 2016. arXiv: 1512.01178 [hep-ph].

[17] J. H. Kim, M. Kim, K. Kong, K. T. Matchev, and M. Park, "Portraying Double Higgs at the Large Hadron Collider", *JHEP*, vol. 09, p. 047, 2019. arXiv: 1904.08549 [hep-ph].

[18] L. Cunqueiro and A. M. Sickles, "Studying the QGP with Jets at the LHC and RHIC", Oct. 2021. arXiv: 2110.14490 [nucl-ex].

[19] J. Casalderrey-Solana and C. A. Salgado, "Introductory lectures on jet quenching in heavy ion collisions", *Acta Phys. Polon. B*, vol. 38, pp. 3731–3794, 2007. arXiv: 0712.3443 [hep-ph].

[20] M. Gyulassy and M. Plumer, "Jet Quenching in Dense Matter", *Phys. Lett. B*, vol. 243, pp. 432–438, 1990.

[21] R. Baier, Y. L. Dokshitzer, A. H. Mueller, S. Peigne, and D. Schiff, "Radiative energy loss of high-energy quarks and gluons in a finite volume quark - gluon plasma", *Nucl. Phys. B*, vol. 483, pp. 291–320, 1997. arXiv: hep-ph/9607355.

[22] R. Baier, Y. L. Dokshitzer, A. H. Mueller, S. Peigne, and D. Schiff, "Radiative energy loss and p(T) broadening of high-energy partons in nuclei", *Nucl. Phys. B*, vol. 484, pp. 265–282, 1997. arXiv: hep-ph/9608322.

[23] Y. Mehtar-Tani, C. A. Salgado, and K. Tywoniuk, "Antiangular ordering of gluon radiation in qcd media", *Physical Review Letters*, vol. 106, no. 12, Mar. 2011.

[24] J. Gallicchio and M. D. Schwartz, "Seeing in Color: Jet Superstructure", *Phys. Rev. Lett.*, vol. 105, p. 022 001, 2010. arXiv: 1001.5027 [hep-ph].

[25] M. Cacciari, G. P. Salam, and G. Soyez, "FastJet User Manual", *Eur. Phys. J. C*, vol. 72, p. 1896, 2012. arXiv: 1111.6097 [hep-ph].

[26] A. Larkoski, S. Marzani, and C. Wu, "Safe Use of Jet Pull", *JHEP*, vol. 01, p. 104, 2020. arXiv: 1911.05090 [hep-ph].

[27] M. Aaboud *et al.*, "Measurement of colour flow using jet-pull observables in $t\bar{t}$ events with the atlas experiment at $\sqrt{s} = 13\,\text{TeV}$", *The European Physical Journal C*, vol. 78, no. 10, Oct. 2018.

[28] T. Sjöstrand *et al.*, "An introduction to PYTHIA 8.2", *Comput. Phys. Commun.*, vol. 191, pp. 159–177, 2015. arXiv: 1410.3012 [hep-ph].

[29] A. C. Ene, A. Jipa, and L.-E. Giubega, "Study of Monte Carlo event generators for proton-proton collisions at LHC energies in the forward region", *Chin. Phys. C*, vol. 43, no. 8, p. 083 001, 2019. arXiv: 1906.02523 [hep-ph].

[30] "Reconstruction and Modelling of Jet Pull with the ATLAS Detector", 2014.

[31] A. J. Larkoski, S. Marzani, G. Soyez, and J. Thaler, "Soft Drop", *JHEP*, vol. 05, p. 146, 2014. arXiv: 1402.2657 [hep-ph].

[32] A. Heister *et al.*, "A measurement of the gluon splitting rate into c anti-c pairs in hadronic Z decays", *Phys. Lett. B*, vol. 561, pp. 213–224, 2003. arXiv: hep-ex/0302003.

[33] W. Busza, K. Rajagopal, and W. van der Schee, "Heavy Ion Collisions: The Big Picture, and the Big Questions", *Ann. Rev. Nucl. Part. Sci.*, vol. 68, pp. 339–376, 2018. arXiv: 1802.04801 [hep-ph].

[34] Z. Yang *et al.*, "Search for the Elusive Jet-Induced Diffusion Wake in Z/γ-Jets with 2D Jet Tomography in High-Energy Heavy-Ion Collisions", *Phys. Rev. Lett.*, vol. 127, no. 8, p. 082 301, 2021. arXiv: 2101.05422 [hep-ph].

[35] B. B. Back, "Studies of multiplicity in relativistic heavy-ion collisions", *J. Phys. Conf. Ser.*, vol. 5, pp. 1–16, 2005. arXiv: nucl-ex/0411012.

[36] J. Adam *et al.*, "Centrality dependence of the pseudorapidity density distribution for charged particles in pb–pb collisions at snn=5.02tev", *Physics Letters B*, vol. 772, pp. 567–577, 2017.

[37] M. Cacciari and G. P. Salam, "Pileup subtraction using jet areas", *Phys. Lett. B*, vol. 659, pp. 119–126, 2008. arXiv: 0707.1378 [hep-ph].

[38] P. Berta, M. Spousta, D. W. Miller, and R. Leitner, "Particle-level pileup subtraction for jets and jet shapes", *JHEP*, vol. 06, p. 092, 2014. arXiv: 1403.3108 [hep-ex].

Appendix A

Pull Vector for low pt jets

As we mentioned in the main text, our journey started in known territory: we settled our systems that would serve as a colour singlet and a colour octet and reproduced the results obtained by the Atlas collaboration in [27]. As the purpose of this dissertation is not the study of the pull vector at low pT, these considerations were not included in the main text. Nevertheless we ought to include them here so as to keep a truthfull record of the steps taken towards the results introduced with this project. That being said we adapted our settings to match the Atlas ones as described before: jets with minimum pT of 25 GeV; jet radius of 0.4; pseudorapidity window ranging from -2.5 to 2.5.

A.1 Pull angle at low pT

In figure A.1 we present the deltaR distribution, which contains information regarding the position of the leading jet towards the subleading jet. Applying the same cuts as described in 2.2.2, one observes that the mass window cut revealed to be the most important cut in terms of making the distributions closer to the truth plot.

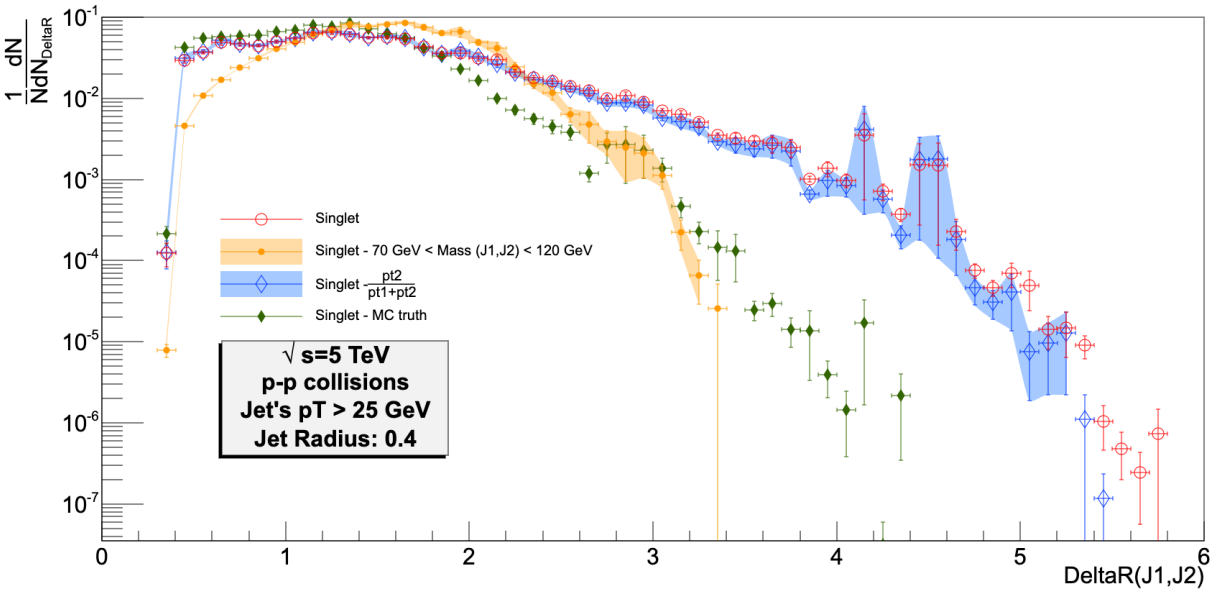

Figure A.1: Study the effect of the cuts in the distance between the 2 prongs at hadron level reconstructed and at the MC truth case. One can observe that the cut that puts the experimental system closer to the Monte Carlo truth distribution is the mass cut, narrowing the window of the W/Z boson.

Let us now analyse the pull angle distribution. In figure A.2 we can compare how close the singlet and octet distributions are to the MC truth distributions.

Additionally in figure A.2a we can also see that the kinematic cuts discussed in the main text have the same effect in the pull angle as for the deltaR distribution: the mass cut brings our observable closer to the MC distribution.

Nevertheless we face an issue at low pt. As one can conclude from figure A.3 one cannot distinguish singlet from octet with our systems at low pT. In [27], by using the $t\bar{t}$ decay channel, they manage to get a singlet system with enough proximity so that they can perform the pull angle studies at low pT. As one cold see from figure 2.12 the two hardest jets are very well collimatted at high-pT. The same does not happen at low pT even by increasing the jet radius. For that we keep this results here only as a matter of record of our steps, since our main concern falls into high-pT jets where our observable and our octet and singlet systems have a good behaviour.

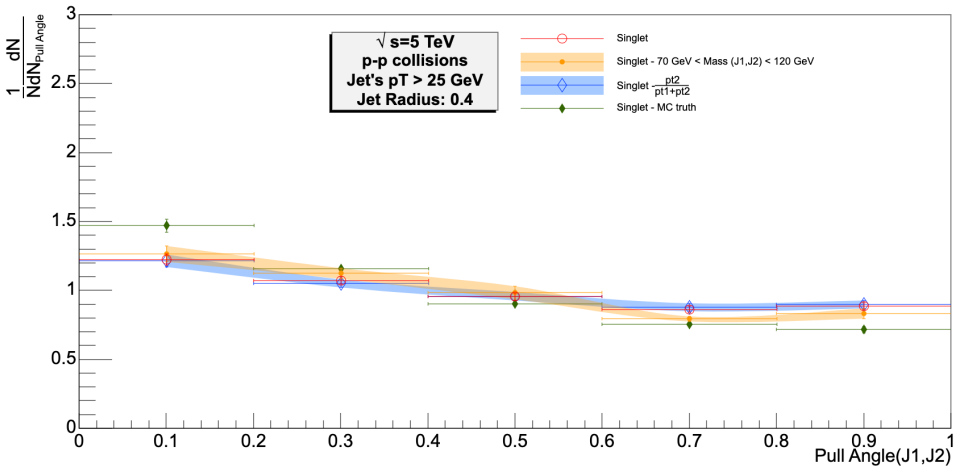

(a) Singlet system versus MC truth and kinematic cuts

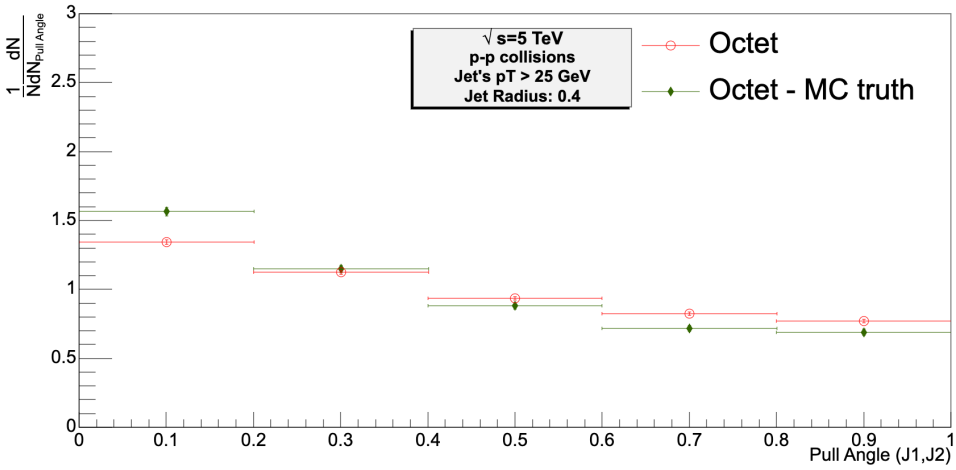

(b) Octet system versus MC truth

Figure A.2: Pull angle distributions for singlet and octet systems and low pT jets

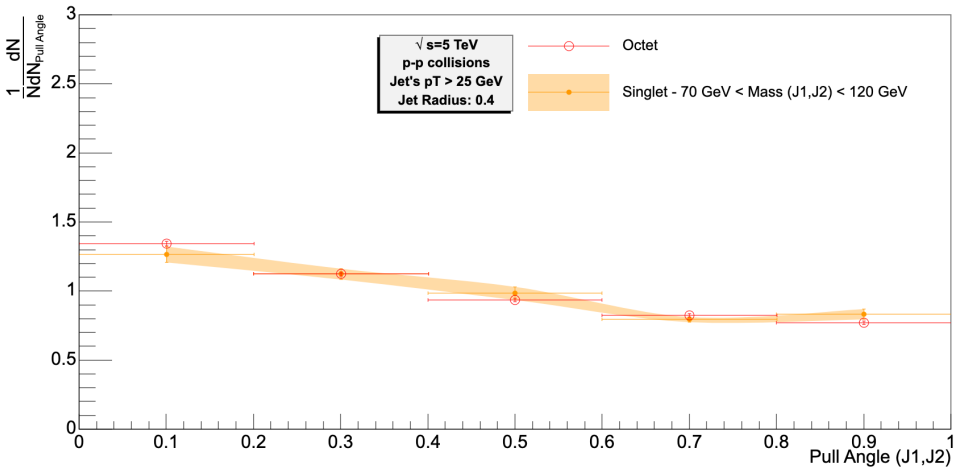

Figure A.3: Pull angle distributions for octet and singlet with the kinematic mass cut